Solar Energy 300 (2025) 113815

Contents lists available at ScienceDirect

Solar Energy

journal homepage: www.elsevier.com/locate/solener

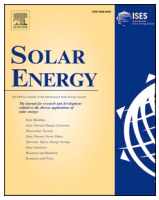

A review on tandem solar cells based on Perovskite/Si: 2-T versus 4-T configurations

Doaa Khodair [a,b], Ahmed Saeed [c,d,*], Ahmed Shaker [e], Mohamed Abouelatta [f,g], Omar A.M. Abdelraouf [e], S. EL-Rabaie [a]

[a] Electronics and Communication Engineering, Faculty of Electronic Engineering, Menoufia University, Egypt
[b] Faculty of Engineering and Technology, Future University in Egypt, Cairo 11835, Egypt
[c] Electrical Engineering Department, Future University in Egypt, Cairo 11835, Egypt
[d] Center of Nanoelectronics and Devices, The American University in Cairo, Egypt
[e] Engineering Physics and Mathematics Department, Faculty of Engineering, Ain Shams University, Cairo 11517, Egypt
[f] Faculty of Engineering, Ain Shams University, Cairo 11517, Egypt
[g] Faculty of Engineering, Egypt University of Informatics, Egypt

ARTICLE INFO

Keywords:
2-Terminal
4-Terminal
Solar cells
Perovskite
Tandem solar cell
Si

ABSTRACT

Perovskite- based solar cells (PVSK-SCs) are a prospective photovoltaic (PV) technology that has the potential to provide a higher power conversion efficiency (PCE) at less expense than the current market standard. The Shockley-Quiesser (S-Q) limit restricts the PCE of single junction cells. Thanks to their ability to surmount this limit through innovative design, tandem solar cells (TSCs) are broadly regarded as the industry's next evolution in PVs. In order to absorb light across a broader spectrum of wavelengths, these architectures combine multiple types of light absorbers with considerably varying band gaps that complement each other's absorption characteristics. The development of halide perovskite (PVSK) absorber material has made it feasible to create TSCs that are more efficient. Perovskites have been applied as a companion in diverse types of TSCs, involving those based on Si and other thin film cells, including CIGS and other perovskite candidates. This review outlines the primary scientific and main engineering issues related to TSC based on PVSK as top sub-cells. The characteristics of TSC technology are discussed, including the potential configurations and device topologies. The advancements in PVSK/Si tandem technologies are reviewed with a specific focus on the mechanically stacked four-terminal (4-T) and the monolithic two-terminal (2-T) multi-junction designs. Lastly, the limitations and challenges that are still limiting the efficiency and commercialization of these PVSK/Si TSC devices are highlighted, along with a roadmap of strategies and future research directions to further increase their PCE.

1. Introduction

Solar cells developed up to date are typically grouped and categorized into four generations [1,2] based on the nature of inorganic photoactive materials utilized in the solar device; (i) first generation (1GEN) solar cells built on Si technologies including both Polycrystalline and Monocrystalline, and on GaAs; (ii) second generation (2GEN) thin-film solar cells (TFSCs) that includes amorphous Si and microcrystalline Si thin films, CdTe, CdS and CIGS solar cells; (iii) third generation (3GEN) solar cells that are based on developing materials and encompasses technologies depending on novel compounds comprising nanocrystalline films, quantum dots (QDs), tandem or multilayers of inorganics grouped to III-V materials, such as GaAs / gallium indium phosphide (GaInP), polymer, DSSCs and perovskite solar cells (PVSK-SCs); and finally (iv) fourth generation (4GEN) solar cells that merge the lower cost and flexibility of thin film polymer materials with the stability of advanced inorganic nanostructures [2]. Due to their efficiency, robustness in manufacturing processes and technologies, remarkable dependability of their materials, and product reliability, single-junction solar cells of the silicon crystalline material dominate the market and are employed in the production of commercial solar modules [3]. However, ongoing research into alternative materials is urging the development of innovative designs and structures aimed at improving the PCE of the developed solar cells.

Several solutions have been established to successfully surpass the S-Q limit and capture the maximum possible number of incident photons

* Corresponding author.

https://doi.org/10.1016/j.solener.2025.113815
Received 20 April 2025; Received in revised form 16 May 2025; Accepted 20 July 2025
Available online 25 July 2025

[4,5]. Incorporating absorber materials with varying Energy band gaps (E_g) into a multi-junction arrangement to complement the absorption characteristics of each other is one of these approaches. This multi-junction design is known as a tandem solar cell (TSC) configuration. This design involves stacking a front sub-cell of wide bandgap (WBG) materials that can absorb high-energy photons with a back sub-cell based on narrow bandgap (NBG) materials that can gather longer wavelength lower-energy photons traversing via the top cell. This configuration allows harvesting a wider range of solar irradiation energy, reducing thermalization losses and maximizing solar spectrum absorption [6,7]. This arrangement expands the solar spectrum coverage, causing an increase in overall efficiency. According to research, compound semiconductor materials like GaInP and GaAs are employed in the manufacturing of III-V multi-junction TSCs showing promising efficient performance [8]. Lately, regarding 3GEN, the metal halide PVSKs (MH-PVSKs) based PV cells have presented a remarkable performance and potential future revolution in PV technology to optimize and yield cost-effective solar electricity and champion power conversion efficiency in TSCs thanks to their extraordinary optical and electrical characteristics, featuring wide carrier diffusion distances, strong light absorption coefficients, heightened charge mobility, and their direct and tunable energy gap [9–11]. These perovskite TSCs generally comprise a front PVSK sub-cell combined with a rear sub-cell, which is often made of Si or another PVSK alternatives having narrower bandgaps. Furthermore, great work has been performed in enhancing the stability of these PV devices, with noticeable advances in encapsulation methods and PVSK composition changes that considerably minimize deterioration in the long run [12]. Regardless of these advances, obstacles remain in research areas. These include, for instance, large-scale production, regularity in thin-film manufacture, and long-term stability [13]. Nonetheless, the potential of PVSK TSCs continues to pique significant interest, both in research and commercial sectors as presented in Fig. 1, which demonstrates the main trends of PVSK-SCs and PVSK-based TSCs over years from 2009 to 2024.

Therefore, in this review, we emphasize recent and topical advancement besides crucial challenges for TSC designs, utilizing PVSK solar cells as the top sub-cell. In this review paper, we present PVSK/Si TSCs, tackling challenges such as fabrication constraints, large-area module fabrication and device stability. As PCEs for laboratory-scale cells steadily improve, there is strong optimism for the progress of highly efficient, low-cost TSCs suitable for commercial usage. Referring to Fig. 2, the review is consolidated as follows: Following the introduction, in section 2, we introduce the background of MH-PVSK materials and the single-junction device structures. Subsequently, the characteristics of TSC technology are discussed, including the potential configurations and device topologies. Next, we explore the advancements in PVSK/Si TSCs with a detailed focus on the mechanically stacked 4-T and the monolithic 2-T multi-junction configurations. Then, the limitations and challenges that are still limiting the efficiency and commercialization of these tandems are highlighted, along with a roadmap of strategies and future research directions to further enhance their output efficiency. Finally, the conclusions of our review paper are presented.

2. Background of halide perovskite materials and single-junction devices

2.1. Crystalline structure of halide perovskite

Perovskite materials typically have the structure of the generic form ABX_3 with varying compositions and a similar crystalline structure, where A and B represent a mixture of various organic and inorganic cations, while X is a smaller halide anion (commonly oxide) that bonds to A and B. As shown in Fig. 3, the molecular structure of the organic halide PVSK follows the ABX_3 configuration. To form a cuboctahedron, the A cation (methylammonium, $CH_3NH_3^+$, MA^+, or formamidinium, $CH_3(NH_2)_2^+$, FA^+) in a PVSK's unit cell is bordered by 12 X anions (Chlorine (Cl^-), Bromine (Br^-), or Iodide (I^-), or existence of multiple

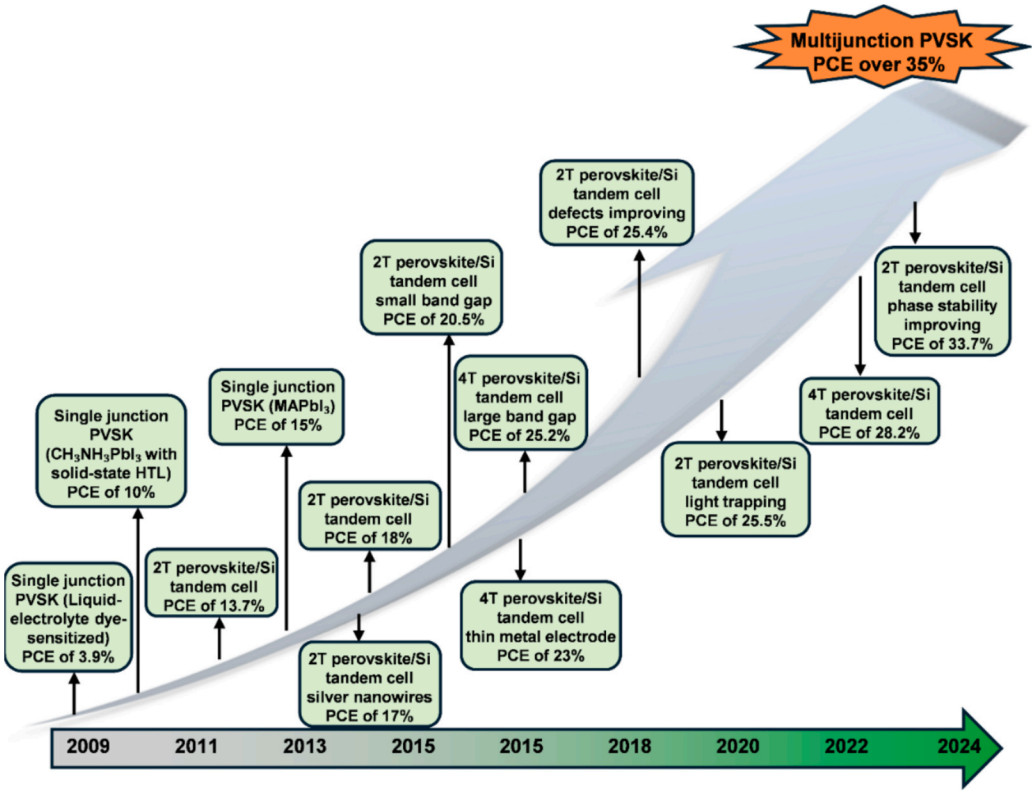

Fig. 1. Main trends of PVSK-SCs and PVSK-based TSCs over years from 2009 to 2024.

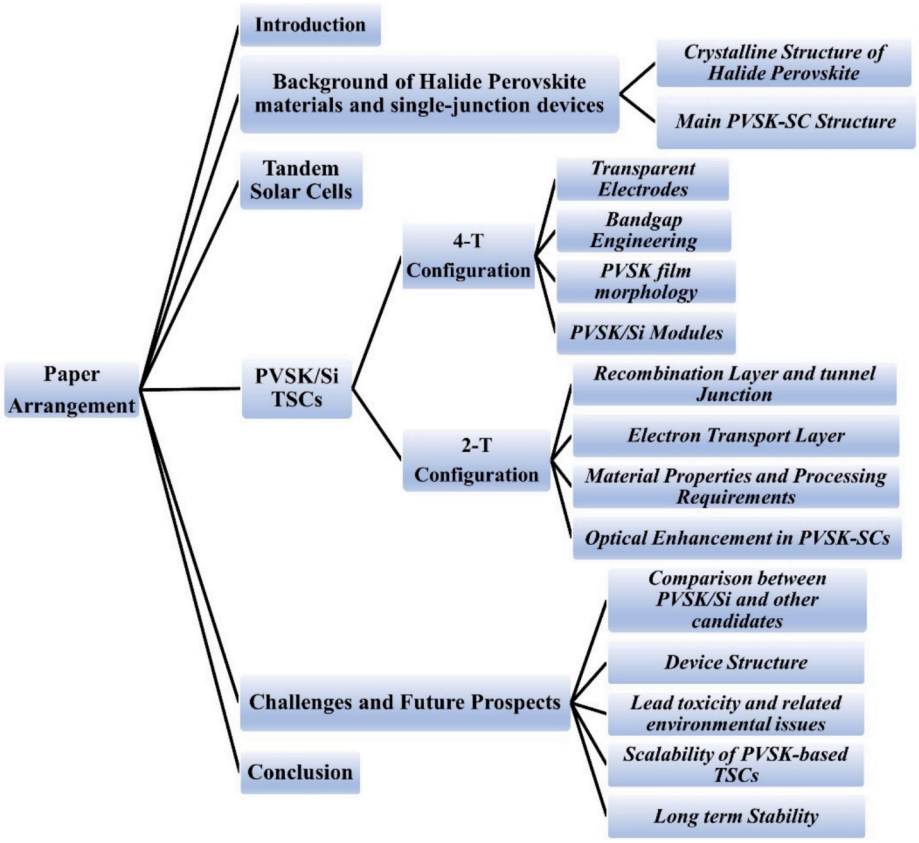

Fig. 2. Arrangement of sections included in this review paper.

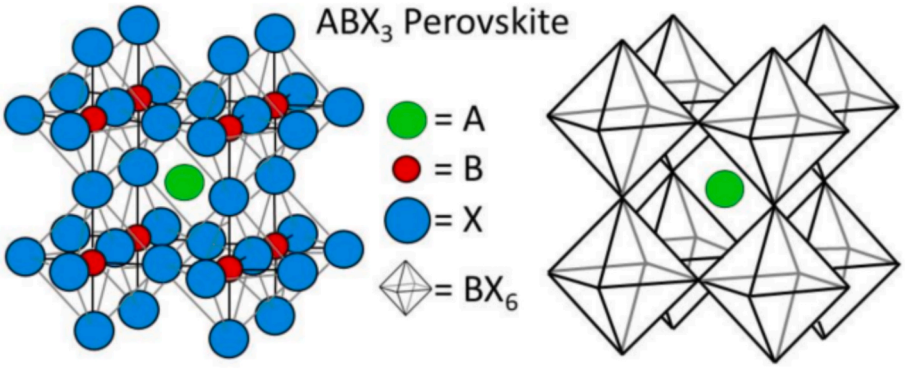

Fig. 3. Crystal lattice structure of the ABX_3 PVSK structure [14].

halogens). The B cation (Pb_2^+, Sn_2^+, etc.) is bordered by six X anions creating $[BX_6]^{4-}$ octahedral. The octahedra formed by B and X are interconnected, creating a stable 3D network configuration.

One of the primary grants of the PVSK structure is its capability to incorporate elements that exhibit a great variation of probable amendments and variants of the configuration [15]. For example, A and B will be divalent and trivalent if X is oxygen (O^{2-}). While, if X is a halogen anion (Cl^-, Br^-, I^-), A and B can be monovalent and divalent, respectively [16], which offers an excellent prospect to readily adjust the material's characteristics, like its bandgap energy. The ion sizes utilized in PVSKs have a strong role in shaping the final structure and its stability [17]. A dimensionless value termed the Goldsmith tolerance factor (t) defined by:

$$t = \frac{r_A + r_X}{\sqrt{2}(r_B + r_X)} \quad (1)$$

It is a successful and widely utilized ratio [18] applied to guess the formability of several forms of PVSKs where, r_A, r_B and r_X are the radii of monovalent cation, divalent metal cation, and monovalent halide anion. It measures the stability of the crystal and its deformability.

Further, PVSK structure formation limit ranges from t equals 0.8 to 1. With upper limit 1, the perovskite projecting an ideal cubic structure fit [17]. Additionally, in case of tolerance factor less than 1 approaching the 0.8 lower limit, symmetry is lost, and the configuration will be deformed because of the tilting of the BX_6 octahedra which in turn will impact the electrical characteristics. While tolerance factors greater than one imply that the cation is too big to suit into the site, preventing the production of perovskite. This shows the importance of taking care of this factor when designing and developing novel materials for PVSK-SCs. Deviations from the indicated range may lead to other alternative and various structures with different characteristics not as same as the perovskite's properties.

Moreover, the stability and distortion of PVSK can be evaluated using the factor (μ), as defined by Equation (2), which is another key factor influencing PVSK formation.

$$\mu = \frac{r_B}{r_X} \tag{2}$$

The tolerance factor (ranging from 0.81 to 1) and octahedral factor (from 0.44 to 0.89) are projected to contribute to the formation and development of a robust PVSK structure for halide perovskites [19].

Because the semiconducting lead metal halides with adjustable bandgaps are the most efficient perovskites, their crystal family has considerable potential for usage in a broad range of nanotechnology applications, incorporating nanostructured PV cells. Indeed, due to its exceptional photon absorption efficiency, interest in PVSK-SCs has surged recently [2]. It was quickly obvious that PVSKs are exceptionally versatile materials that can achieve high conversion efficiencies at low prices due to their comparatively simple production and manufacturing techniques. Furthermore, as mentioned before, the extended carrier separation lifetime, strong absorption spectrum, greater mean free path of charge carriers, and other properties make perovskite materials suitable for the construction of PV devices [15]. The initial experimental endeavor of a PV cell based on the organic–inorganic lead halide PVSK chemicals $CH_3NH_3PbI_3$ and $CH_3NH_3PbBr_3$ was reported in the literature by Akihiro Kojima and coworkers in 2009 [20] with an efficiency of 3.81 % and an open-circuit voltage (V_{OC}) of 0.96 V. In comparison to crystalline Si solar cells, metal halide PVSK-SCs have undergone remarkable progress over the past ten years, achieving a verified PCE of over 25 % because of composition engineering, PVSK film growth control and PVSK/transport layer interface engineering as summarized in Table 1 [21–27].

2.2. Main PVSK-SC structure

Efficient PVSK-SCs have the potential to be an interesting and desirable approach for commercial solar technology manufacturing. It is vital to note that the structure of the device, as well as the kind and crystalline structure of PVSK and charge transporting materials, all play significant responsibilities in determining the functioning and durability of the device. Basically, the cell structure of PVSK-SCs consists of a photoactive film inserted between an electron transport layer (ETL) (which is accountable for transferring the electrons produced in the PVSK absorber to the corresponding electrode) and a hole transport layer (HTL) (which is accountable for transferring the holes created within the PVSK to the other electrode), a transparent conductive oxide (TCO) (which may be materials like FTO, or ITO as an anode and a metal contact (cathode)). PVSK-SCs are separated into two groups, the normal n-i-p and inverted p-i-n structures [28]. These types are presented in the schematic construction of the device demonstrated in Fig. 4. For both configurations, the incident solar radiation penetrates the PVSK photoactive layer via the transparent conductive oxide. Then, the light generated carriers coexist in the PVSK absorber and transported through the ETL and HTL layers, respectively, towards the selective electrodes. By varying the material composition, PVSKs may be adjusted to react to different spectrum hues. To ensure adequate carrier collection, the materials managed in ETL and HTL should have the appropriate band alignment [29].

Table 1
Variations in the structure and composition of single-junction PVSK-SCs as indicated by the conversion power efficiency record.

Perovskite cell based	PCE (%)	Year	Reference
$CH_3NH_3PbI_3$	3.81	2009	[20]
CH_3NH_3I–PbI_2*–DMSO*	16.5/16.2[a]	2014	[21]
$MAPbBr_3$ + $FAPbI_3$	18.0/17.9[a]	2015	[22]
HTAB*$_{0.3}$($FAPbI_3$)$_{0.95}$($MAPbBr_3$)$_{0.05}$	22.8/22.7[a]	2019	[23]
FAI + FABr + PbI_2	23.32[a]	2019	[24]
$FAPbI_3$ + $MAPbBr_3$ + PbI_2 + MACl	25.2[a]	2021	[25]

* DMSO: γ-butyrolactone and dimethylsulphoxide.
* PbI_2: Lead Iodide.
* HTAB: *n*-hexyl trimethyl ammonium bromide.
[a] Certified power conversion efficiency.

Both organic and inorganic materials can be utilized in the transporting layers. In general, organic HTLs have high cost. The most commonly used HTL, Spiro-OMeTAD [30] is 10 times more expensive than Platinum and Gold. Some research implies that organic HTLs actively assist in the degradation process, leading to the low stability of PVSK-SCs [31]; so, the future growth of PVSK-SCs necessitates careful choice of the HTL. Inorganic HTLs appear to be a viable prospective substitute because of their lower price and ease of synthesize with better stability [31]. Inorganic p-type semiconductors such as QDs and nanocrystals contribute to the improvement of PVSK-SCs performance.

Before choosing any material, an acceptable and appropriate energy level matching with the perovskite is essential. Two main factors must be taken in consideration when selecting appropriate HTL materials [32], first, adjustment of the highest occupied molecular orbital (HOMO) energy level in the inorganic p-type semiconductors to a proper position and hole collection to obtain optimum current density [33]. Secondly, a less particular contact between PVSK and HTL must be taken in consideration aiming to decrease the carrier recombination, as it impacts the V_{OC} of the cell by disturbing the splitting of the quasi Fermi-energy levels of the PVSK absorber material [30]. Graphene oxide (GO), CuSCN, CuI, Cu_2O, NiO_x and more are considered to be different potential materials that can be employed as inorganic HTLs [31].

Also, the ETL makes a significant contribution to efficiency and stability. In order to satisfy effective charge extraction, the conduction band (CB) of the ETL must be less than that of the absorber, whereas the valence band (VB) of the absorbing material should be higher than that of the ETL [34]. In addition, the ETL/PVSK interface is critical to cell performance, as inadequate band alignment between the ETL and the PVSK layer can strengthen carrier recombination and negatively affect series and shunt resistances. To overcome these disputes, high carrier mobilities and good band alignment materials ought to be carefully selected in order to enhance electron injection and hole blockage capabilities at the ETL/PVSK interface, leading to high short circuit current density (J_{SC}) and boost cell performance [35]. Although TiO_2 is the most widely employed ETL due to its better stability, the fact that it aids the ion immigration process and their needs for high annealing temperature, that leads to the cell damage and performance degradation, prompts the researchers to seek an alternative such as ZnO, CdS, PCBM, and SnO_2 [36]. SnO_2 is considered now the most preferred ETL material because of its wider bandgap of 3.6–4.1 eV and deeper CB than TiO_2. Moreover, SnO_2 has a greater mobility of 240 cm^2/V, and higher optical transmittance and conductivity besides its low temperature production utility [36]. This improves the collection and transport of charge carriers. Properties and features of different potential materials for ideal ETLs and HTLs to construct more efficient PVSK-SCs devices can be found in [13].

Another critical component in the operation of a PV cell is the transparent conductive electrode (TCE) with proper transparency and conductivity features [37]. As a good balance between conductivity and transparency is required for an effective TCE, the choice of an adequate TCE is influential [38]. It was found that even with heterojunction topologies, the improvement in PCE is significantly restrained by carrier recombination procedures in the perovskite itself or interfaces between films. Hence, it is imperative to reduce the rates of carrier recombination within the PVSK layer to enhance the PCE of the cell. So, improvements and enhancements in the fabrication processes is a strategy to decrease and reduce defect sites in the perovskite layer [39,40]. Compositional engineering [22,41] and alternative architecture design [42], are other approaches that have been investigated to lower the recombination losses.

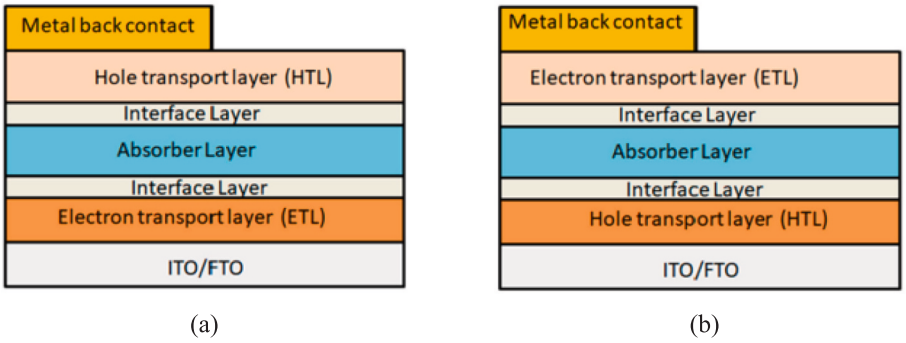

Fig. 4. Demonstration of the two fundamental types of PVSK-SC structure: (a) n-i-p structure (normal type), (b) p-i-n structure (inverted type) [10].

3. Tandem solar cells

Due to the inherent limitation in the maximum PCE attainable by single-junction cells according to the Shockley-Queisser's constraint, alternative approaches and different routes are being explored to augment the output power of PV cell devices for exceeding the S-Q limit for the single p-n junction. TSC architectures, also known as 'Multi-junction devices', are considered one of the approaches that have attracted significant interest for developing cost-effective and efficient PVs owing to their efficient aptitude to absorb a wide range of light spectrum, hence, achieving superior output PCE and better stability among the time [13]. As mentioned before, this topology entails the blend of several materials that complement absorption properties of each other [8].

A TSC can be constructed in distinct ways, with each approach depending on how the junctions that connect the front and back cells are electrically linked. Based on the physical integration of the sub-cells, TSCs can be classified as either monolithic Two-terminal (2-T), Three-terminal (3-T) or Four-terminal (4-T) tandems [43]. Among these classifications, the two famous widely used designs are the monolithic 2-T and mechanically stacked 4-T structures. These arrangements differ significantly from both electrical and construction perspectives, as illustrated in Fig. 5.

In two-terminal configuration, a second sub-cell is built in monolithic design and stacked on top of the first sub-cell. This necessitates precise manufacturing compatibility and current matching through both cells, which are coupled in series and joined monolithically via tunnel junctions [44] or thin recombination layers, such as ITO or ultra-thin metal [45,46]. Two external electrical contacts are required for the 2-T tandem configuration, and one of them must be semitransparent to ease the light passing through the device. For the 2-T TSCs, both sub-cells are electrically connected, and the two-terminal tandem voltage ($V_{OC,2\text{-}T}$) established is the sum of the voltages acquired by top and rear cells as shown in Equation (3). By similarity, the two-terminal tandem current ($J_{SC,2\text{-}T}$) and the two-terminal tandem fill factor ($FF_{2\text{-}T}$) controlled by Equations (4) and (5) respectively, are limited by the minimal value established between front and rear sub-cells.

$$V_{OC,2-T} = V_{OC,Top} + V_{OC,Bottom} \tag{3}$$

$$J_{SC,2-T} = \min[J_{SC,Top},\ J_{SC,Bottom}] \tag{4}$$

$$FF_{2-T} = \min[FF_{Top}, FF_{Bottom}] \tag{5}$$

where $V_{OC,2\text{-}T}$, $V_{OC,Top}$, $V_{OC,Bottom}$ indicates for the tandem, front and rear voltage, respectively. In addition, $J_{SC,2\text{-}T}$, $J_{SC,Top}$, $J_{SC,Bottom}$ are regarded as tandem, front and rear currents, respectively. $FF_{2\text{-}T}$, FF_{Top}, FF_{Bottom} represents tandem, front and rear FFs.

In Four-terminal configuration, a mechanical stacking optically links the two electrically isolated cell devices that are made on distinct substrates. Under this tandem design, each sub-cell is attached to an external circuit and works individually. Thus, this enables independent optimization for each cell as the output powers are separately extracted to efficiently merge their corresponding output power. According to the 4-T TSCs, as the current matching criterion is not compulsory, where the

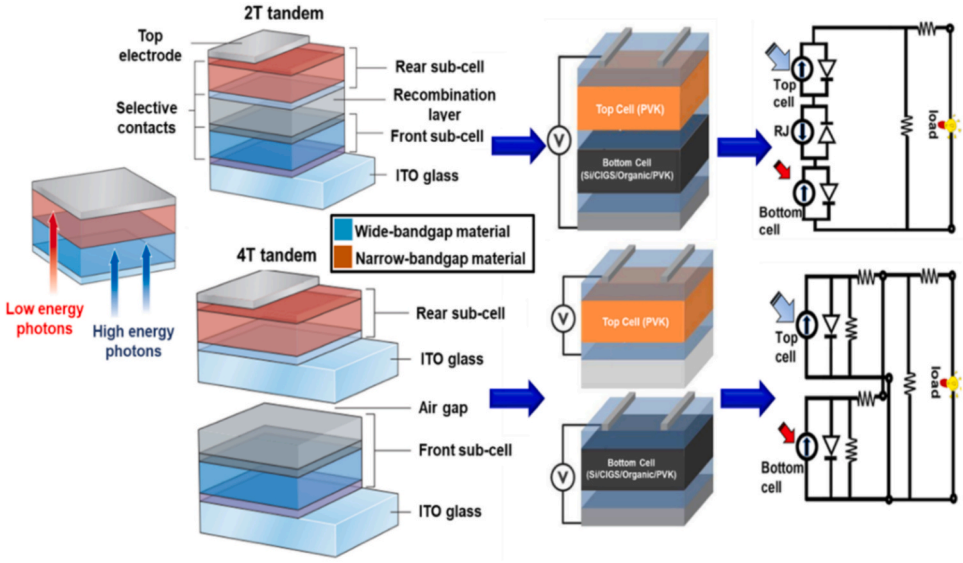

Fig. 5. Two-terminal and Four-terminal TSCs strictures with their equivalent electrical circuit diagram [19].

two cells are stacked mechanically as two isolated units, the total 4-T tandem PCE ($PCE_{4\text{-}T}$) is the sum of the front and rear cells as declared in Equation (6).

$$PCE_{4-T} = PCE_{Top} + PCE_{Bottom} \quad (6)$$

where PCE_{Top} and PCE_{Bottom}, represent the PCEs of front and rear sub-cells respectively.

The fewer number of semitransparent electrical contacts needed in the 2-T design results in a slight improvement in overall efficiency. This is due to reduced reflection and parasitic absorption compared to the 4-T design, which requires 4 contacts per TSC, with 3 of them ought to be semi-transparent to let light to traverse through the sub-cell. However, despite the arrangement of series-connected 2-T TSCs considered the most required [47], processing of these tandem cells is complex and more challenging in realizing a well-matched combination of front and rear devices, producing a recombination interlayer with minimum losses between the corresponding sub-cells, and guaranteeing efficient optical assessing within the TSC construction. The introduction of series–parallel tandem configurations [48,49] offers a practical method to unite the output power of two cells while preserving performance levels similar to 4-T schemes in terms of overall energy yield. This is accomplished by individually linking the front and rear cell strings and subsequently attaching the voltage-matched strings in parallel. The features and differences between 2-T and 4-T TSC designs are reviewed in Table 2.

4. PVSK/Si TSCs

Over recent years, PVSK-SC performance has surpassed 25 % efficiency due to advancements in low-temperature synthesis of perovskite films and improved interface and electrode materials [50]. Organic-inorganic halide perovskites are excellent candidates for TSC applications, thanks to their tunable bandgaps, strong absorption edge, and solution processability. These properties make them ideal for combining with low-bandgap absorber materials like Si, as discussed in the following subsections. Fig. 6 schematically illustrates the recent PCE advancements for 2-T and 4-T tandem configurations employing PVSK/Si TSCs and the prospective for Si and PVSK single junctions.

Notably, silicon arrays and modules dominate over 90 % of the solar PV market owing to their high PCE, superb stability, optimal bandgap energy ($E_g = 1.12$ eV) [54], and low industrial production cost at scale [55]. Cost-effective TSCs combine the inexpensive production of PVSK with the stability of commercial Si cells, which absorb light across 300–1200 nm. Si cells, frequently used as rear sub-cells in TSCs, capture lower-energy photons transmitted through the front cell, enabling broader light spectrum utilization [56]. Pairing a rear Si cell with a top PVSK-SC offers a promising approach for low-cost tandem multijunction designs, as their complementary absorption properties span a wider wavelength range. The combination of 2-T and 4-T PVSK/Si-based TSCs is a hopeful strategy to enhance efficiency and solar spectrum use, leading to superior performance. However, successful integration requires careful material compatibility and device configuration optimization. In this section, we will review the advancements of both 4-T and 2-T PVSK/Si-based TSCs.

Table 2
Characteristics of 2-T and 4-T TSCs.

2-T Configuration	4-T Configuration
The necessity for current matching between the two dissimilar bandgaps series-connected cells.	Not limited by matching current and series connection between both sub-cells.
Front and bottom cells are directly integrated.	Fabrication of front and bottom cells is independent.
Optical coupling is needed.	Optical coupling is required.
Difficulties in manufacturing owing to issues of recombination interlayers with minimum losses between the sub-cell and optical organization.	It is relatively easy to fabricate because the sub-cells are electrically independent and work individually to obtain the maximum power.
Fewer processing phases are needed.	Easier in the maintenance process than 2-T TSCs.
Less parasitic absorption from the glass substrate.	More optical losses owing to parasitic absorption.
TSC's longevity depends on the performance of the front PVSK-SC.	The device's overall efficiency is insensitive to the solar spectrum.
The potential for commercialization due to the low-cost manufacturing.	High-cost fabrication makes commercialization not feasible.

4.1. 4-T configuration

4.1.1. Transparent electrodes

The development of transparent electrodes plays a central role in improving the performance and efficiency of PVSK/Si TSCs, particularly in a 4-T configuration. However, achieving high transparency while maintaining electrical conductivity and stability poses significant challenges, as the deposition processes can damage the delicate absorber layers. To address these challenges, researchers have explored several transparent conductive oxides (TCOs), buffer layers, and alternative electrode materials, optimizing their integration into TSCs.

Sputter-deposited TCOs with buffer layers like molybdenum oxide (MoO_x) can be utilized to protect the PVSK layer from damage occurred while depositing the TCO film [57]. For example, **Löper et al.** [58] employed ITO with a MoO_3 buffer to shield against sputtering damage, marking an early attempt at MH-PVSK/c-Si TSCs. The first 4-T PVSK/Si TSC device, featuring $MAPbI_3$ as the front sub-cell and a Si heterojunction (SHJ) as the rear sub-cell, is displayed in Fig. 7**(a)**. Given a transparent MoO_x/ITO contact, the 4-T TSC achieved a combined efficiency of 13.4 %. The external quantum efficiency (EQE) spectrum of this tandem system is illustrated in Fig. 7**(b)**.

To prevent damage to underlying layers, **Bailie et al**. [59] employed a solvent-free approach, mechanically transferring transparent silver (Ag) nanowires (NWs) from flexible polyethylene terephthalate (PET) onto Spiro-OMeTAD surfaces. The AgNWs film achieved over 90 % transmission between 530–730 nm, with the semitransparent top sub-cell exhibiting a PCE of 13 % and peak transmittance of 77 % at 800 nm. A 4-T tandem cell combining $CH_3NH_3PbI_3$ (top) and multi-crystalline Si (mc-Si) (bottom) reached a PCE of 17 % (top: 12.7 %, bottom: 4.3 %). Nevertheless, Ag diffusion into charge transport layers (CTLs) and PVSK results in silver iodides, degrading the device [60]. Thus, selecting stable electrodes like Cu or Au is critical. Chen et al. [61] demonstrated superior performance using an Au (7 nm)/Cu (1 nm) bilayer electrode (Fig. 8**(a)**). A 4-T tandem with this configuration reached a combined PCE of 23 % using an infrared-enhanced SHJ cell.

Buffer layers like MoO_x and V_2O_5, deposited by low-temperature thermal evaporation, without post-annealing, protect CTLs during sputtering. In contrast, ETLs like ZnO and TiO_2 need post-annealing at high temperatures [62–64]. **Bush et al.** [62] utilized a solution-processed amorphous aluminum-doped zinc oxide (AZO) nanoparticle film as a sputtering buffer, as seen in Fig. 8**(b)**, enabling a semi-transparent PVSK-SC with a conversion efficiency of 12.3 %. When paired with a monocrystalline Si cell (PCE: 17 %), the 4-T tandem achieved 18 % efficiency. Further, Duong et al. [63] introduced PVSK-SCs with ITO directly sputtered onto the Spiro-OMeTAD HTL in an n-i-p design, eliminating the buffer layer. Their methylammonium PVSK ($MAPbI_3$) device achieved 12 % PCE and over 80 % transmittance in the 800–1000 nm range. Using a 105 nm ITO film with 44 sq^{-1} sheet resistance removed the need for grid fingers, improving current density. **Jaysankar et al.** [65] optimized 4-T PVSK/Si tandem modules for light management. They textured the top glass of PVSK-SCs with inverted pyramids to reduce reflection losses, a major issue in planar PVSK/Si TSCs. Replacing the airgap between the CsFAPbIBr PVSK and IBC Si cells with a refractive index matching layer (IML), as shown in Fig. 8**(c)**, improved NIR light transmission.

To minimize optoelectronic losses relevant to tandem structures,

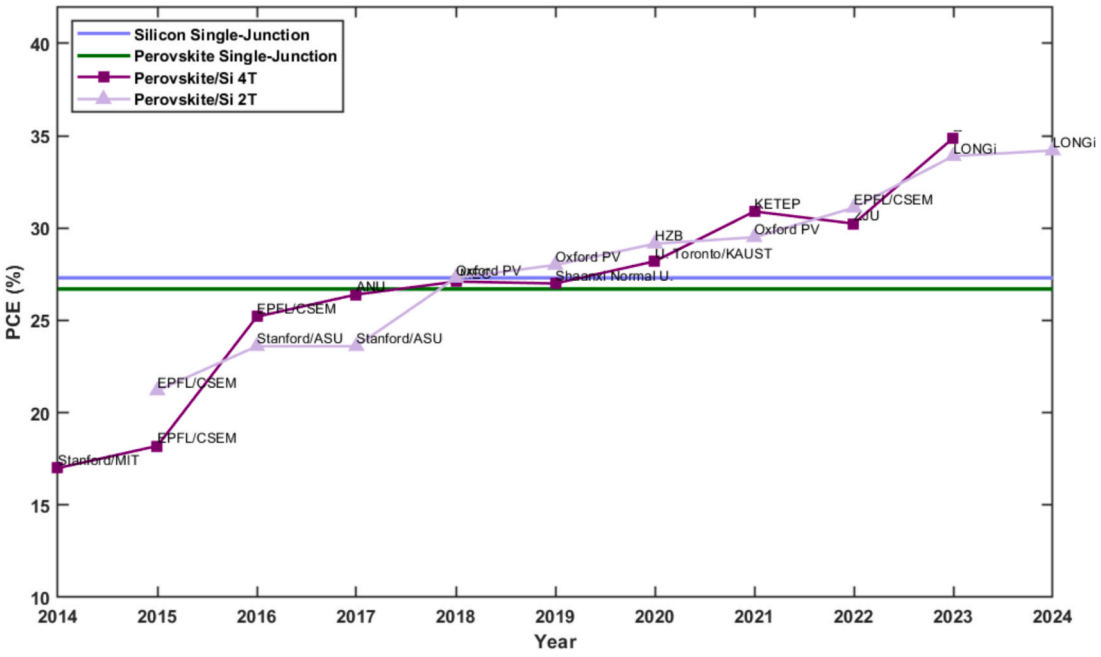

Fig. 6. Efficiency evolution for PVSK/Si TSCs in 2-T and 4-T multijunction design with Si material as a bottom sub-cell. Data is extracted from published articles, and the abbreviation denotes the company, university or institute that reported the PCE [51–53].

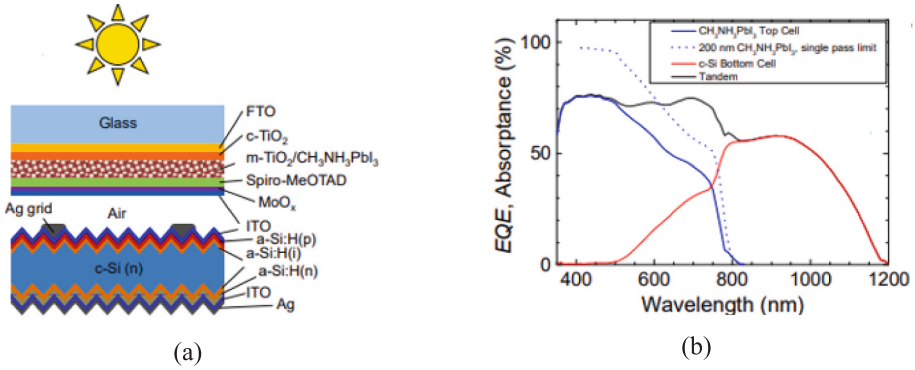

Fig. 7. (a) Schematic representation of the 4T PVSK/Si TSC [58], (b) EQE absorption for the corresponding tandem device [58].

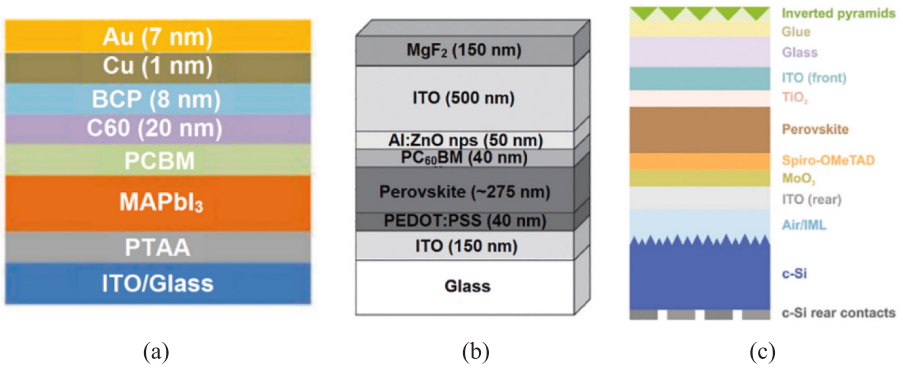

Fig. 8. (a) Schematic of inverted PVSK with (1 nm Cu/7 nm Au) electrode [61], (b) illustration of the semitransparent PVSK with AZO buffer layer [62], and (c) 4-T tandem configuration with inverted pyramid textures and refractive IML [65].

CuSCN was chosen as the HTL and antireflective layer between the TCO electrode and the photoactive PVSK layer as addressed in [66]. This approach reduced optical losses to a minimum due to low parasitic absorption and better matched refractive index of CuSCN compared to PVSK materials in the NIR region. Also, by utilizing a transparent MoO_3/Au/MoO_3 electrode, a high-performance 4-T PVSK/c-Si tandem device was developed, achieving transmittance at extended wavelengths [67]. Using biomimicking elastomeric petals (BEP) (Fig. 9) as a light-trapping

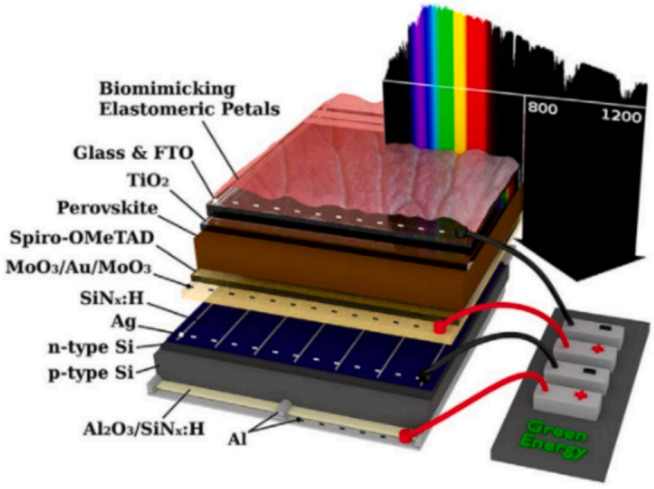

Fig. 9. Device schematic of the four-terminal PVSK/c-Si TSC [67].

film, a PCE of 22.4 % was achieved. In another attempt, which was based on thermally evaporated MoO_3/Au/MoO_3 electrode, a total efficiency of 27 % was recorded in a 4-T tandem with an SHJ cell [68].

4.1.2. Bandgap engineering

To develop 4-T TSCs with silicon, PVSKs must have an optimized bandgap to maximize efficiency. Since $MAPbI_3$, with $E_g = 1.55$ eV, is not the best choice for PVSK/Si multi-junctions, researchers have explored alternative materials with higher bandgaps. **Werner et al.** [69] developed semitransparent PVSKs with bandgaps tuned for tandem applications, achieving 14.5 % efficiency for 1 cm^2 and 16.4 % for 0.25 cm^2 using a two-step deposition method. After mechanical stacking with SHJ cells, they obtained PCEs of 23 % and 25.2 %, with a 20.5 % efficient large-area PVSK/SHJ tandem. To further address the bandgap mismatch, researchers have investigated bromide substitution for iodide to increase E_g, but phase segregation under light exposure remains a challenge, leading to efficiency losses [70–74]. Other alternatives have also been proposed to achieve stable higher-bandgap materials suitable for tandem integration. For instance, rubidium was introduced into a FA/MA/Cesium perovskite (CsFAMA) system to achieve a 1.73 eV bandgap perovskite [75]. The semitransparent cell demonstrated 84 % transparency and a PCE of 16 %. When combined with a 23.9 % IBC silicon cell, the four-terminal multijunction yielded 26.4 % PCE.

Additionally, **Snaith et al.** [76] developed efficient 4-T TSCs by integrating SHJ cells with a mixed cation (FA/Cs) MH-PVSK solar cell, $FA_{0.83}Cs_{0.17}Pb(I_{0.6}Br_{0.4})_3$, having an E_g of 1.74 eV. They fabricated PVSK-SCs with V_{OC} of 1.2 V and PCEs of 17.1 % and 14.7 % utilizing small and large areas, respectively. Integrating these PVSK-SCs with a 19 % efficient Si cell, the TSC achieved a PCE >25 %. A triple cation $Cs_{0.06}(MA_{0.17}FA_{0.83})_{0.94}Pb(I_{0.83}Br_{0.17})_3$ PVSK was integrated into a TSC with an industrial-grade n-type monocrystalline PERT Si solar cell [77]. The produced 4-T TSC showed high visible light absorption and 80 % transmittance from 800 to 1100 nm, while the total achieved efficiency of 26.6 % is among the highest reported for 4-T PVSK/Si TSCs.

4.1.3. PVSK film morphology

Notably, achieving high-efficiency PVSK/Si TSCs requires optimizing perovskite film morphology in order to reduce defects thereby reducing recombination losses. In this context, advanced fabrication procedures have been developed to advance film quality to enhance overall device performance. **Sargent's group** [78] improved PVSK films using solvent extraction, resulting in a dense, smooth morphology and increased electron diffusion length. A 1.63 eV semitransparent PVSK-SC achieved a PCE of 19 % with 85 % transparency in the NIR. In a 4-T PVSK-SHJ structure, the device reached 28.2 % stabilized PCE at 0.049 cm^2 and 25.7 % at 1 cm^2.

To accomplish efficient and stable PVSK/silicon tandems, it is highly desirable to mitigate the electronic defects at the grain boundary. In [79], the authors applied a synergistic passivation strategy for $Cs_{0.05}FA_{0.82}MA_{0.13}Pb(I_{2.86}Br_{0.14})$ PVSK material. The crystallization process was modulated by the incorporation of a small quantity of NaF into PVSK precursor solution, resulting in large crystal grains. In the interim, a thin 2D PVSK film was fabricated on the surface of the 3D PVSK layer through the solution coating of PEAI. This approach passivates the surface defects and enhances the stability of perovskite films. For further boosting the performance of WBG-PVSK solar cells, designing surface engineering strategies were considered, as the method developed by Xipeng et al. [80]. The recent research focused on developing a surface reconstruction technique of the 1.67 eV wide bandgap PVSK films which involved wet nano-polishing to remove the defect-rich crystal surfaces followed by the passivation of the newly exposed high-crystallinity surface. This methodology has the potential to enhance the charge collection and impede the ion migration of WBG perovskites by refreshing the PVSK/electron-transporter interface and releasing the residual lattice strain of the bulk perovskite film.

4.1.4. PVSK/Si modules

Scaling up while maintaining efficiency is challenging due to increasing sheet resistance and short circuits in large-area devices. Numerous efforts have been dedicated to developing PVSK/Si modules [65,81–84]. **Jaysankar et al.** [81] described a scalable 4-T PVSK/c-Si tandem module, stacking a 4 cm^2 semitransparent $CH_3NH_3PbI_3$ PVSK solar module on an IBC c-Si cell, as illustrated in Fig. 10**(a)**. Optimized transparent contacts and module design resulted in PCEs of 22.6 % (0.13 cm^2) and 20.2 % (4 cm^2). Upscaling of PVSK/Si TSCs was also investigated by using a hybrid processing method to deposit mixed cation mixed halide PVSKs [85,86] **(see** Fig. 10**(b))**. In this experimental endeavour, the top cell uniformly covered the micrometer-sized pyramid texture of the rear cell **(**Fig. 10**(c))**. The bottom cell used 250 μm thick p-type wafers with 1 O cm resistance and a-Si heterojunction surfaces [87]. The back electrode had evaporated Ag, while the front was coated with 20 nm ITO. Initial results for a 1 cm^2 area showed 25.2 % infiltration of the inorganic scaffold via spin coating. Screen-printing of low-temperature Ag paste for front metallization in large areas (102 × 102 mm^2) yielded 22.5 % efficiency and a V_{OC} of 1771 mV for cells with a total area of 104 cm^2. Spin coating proved effective for growing PVSK on planar surfaces, though inhomogeneities were identified via photoluminescence. To address this, inkjet printing and spray coating showed promising results, with potential efficiencies up to 28 % for large-area textured PVSK/Si tandems with printed metallization [85]. Recent progress and properties of four-terminal perovskite/Si TSC devices are provided in Table 3.

4.2. 2-T Configuration

Unlike 4-T configurations, where each sub-cell operates independently, 2-T tandems necessitate current matching between the sub-cells, making absorber optimization a critical design factor. Recent advancements in material engineering, transparent electrode integration, and interface optimization have substantially improved the performance and stability of 2-T PVSK/Si TSCs. The following discussion explores key developments, including absorber tuning, interface engineering, and innovative recombination interlayers, to enhance efficiency and long-term durability.

4.2.1. Recombination layer and tunnel junction

The first 2-T PVSK/Si multi-junction TSC with n^{++}/p^{++} Si tunnel junction was constructed in 2015 [44]. It was formed by plasma-enhanced chemical vapor deposition (PECVD) of n^{++} a-Si:H on n-type Si. The tandem cell used an $MAPbI_3$ absorber layer and TiO_2 as the ETL. This 1 cm^2 TSC achieved 13.7 % PCE at 1.65 V, but performance was

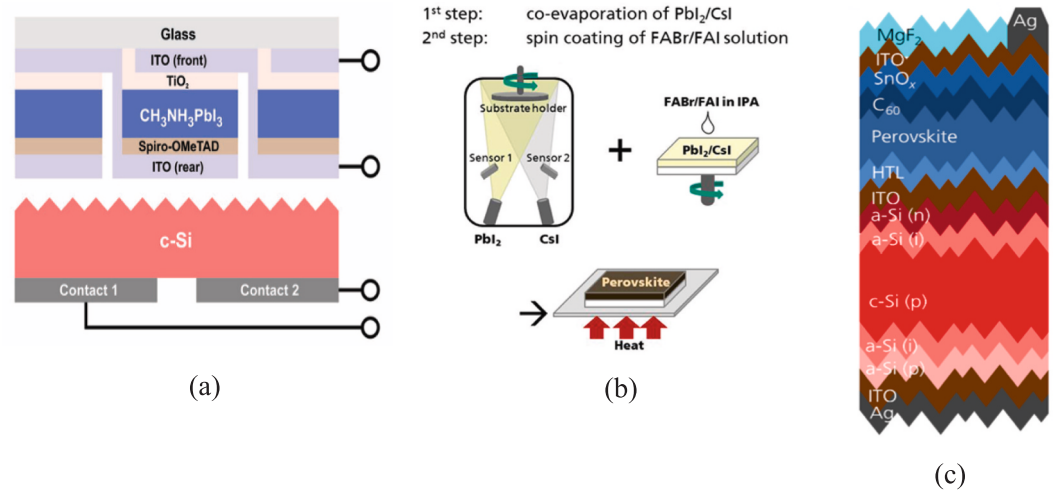

Fig. 10. (a) Module on cell architecture for the four-terminal PVSK/Si TSC [81], (b) Hybrid deposition route used for PVSK-SCs [86], and (c) PVSK/Si TSC with textured structure [85].

Table 3
Summary of Four-terminal configuration PVSK/Si based TSCs progress in recent years.

Top cell				Bottom cell				Filtered Bottom cell				4-T TSC		
J_{sc} (mA/cm^2)	V_{oc} (V)	FF (%)	PCE (%)	J_{sc} (mA/cm^2)	V_{oc} (V)	FF (%)	PCE (%)	J_{sc} (mA/cm^2)	V_{oc} (V)	FF (%)	PCE (%)	PCE (%)	year	Ref.
17.5	1.025	71.0	12.7	29.3	0.582	66.7	11.4	11.1	0.547	70.4	4.3	17.0	2015	[59]
20.6	1.08	74.1	16.5	39.0	0.716	75.9	21.2	12.3	0.679	77.9	6.5	23.0	2016	[61]
16.5	0.652	77.4	12.3	38.3	0.587	75.4	17.0	13.3	0.562	76.2	5.7	18.0	2016	[62]
18.8	0.95	69.0	12.4/12.2[a]	39.1	0.66	76.0	19.6	16.9	0.64	73.0	7.9	20.1	2016	[63]
19.3	1.057	71.6	14.5[b]	38.7	0.718	79.4	22.05	15.5	0.692	79.4	8.5[b]	23.0[b]	2016	[69]
20.1	1.069	76.1	16.4[b]					25.98	0.693	79.5	8.8[b]	25.2[b]		
21.5	1.1	73.5	16.6	41.0	0.72	81.3	24.0	14.2	0.69	81.0	7.9	24.5	2017	[56]
19.4	1.13	70.0	15.4/16.0[a]	41.6	0.71	81.0	23.9	18.8	0.69	80.0	10.4	26.4	2017	[75]
20.0 ± 0.2	7.1 ± 0.06	73.4 ± 1.5	15.3 ± 0.3	41.3 ± 0.04	0.691 ± 0.001	80.6 ± 0.1	23.0 ± 0.01	15.6 ± 0.03	0.674 ± 0.002	81.7 ± 0.1	8.6 ± 0.04	23.9 ± 0.3	2018	[65]
21.0	1.098	74.1	17.1	41.5	0.680	79.5	22.4	17.7	0.674	80.1	9.6	26.7	2018	[66]
23.7	1.06	71.0	17.9	40.2	0.63	75.0	19.1	13.0	0.59	75.0	5.8	22.4	2018	[67]
21.1	1.07	72.3	16.7	–	–	–	–	16.9	0.675	81.3	9.3	26.0	2019	[84]
19.8	1.156	79.9	18.3	41.1	0.708	80.3	23.3	15.6	0.698	80.1	8.7	27.0	2020	[68]
17.5	1.205	76.3	16.1	40.1	0.699	80.1	22.4	18.6	0.675	80.4	10.1	26.2	2020	[88]
19.7	1.16	78.7	18/17.5[a]	41.4	0.69	81.2	23.2	15.6	0.66	80.2	8.2	25.7	2020	[89]
22.3	1.12	77.7	19.0[b]	–	–	–	–	17.2	0.7	76.6	9.2	28.2[b]	2020	[78]
22.4	1.12	66.9	16.5[b]									25.7[b]		
21.9	1.137	79.7	19.8	40.1	0.708	82.5	23.4	14.5	0.698	83.5	8.5	28.3	2021	[90]
23.6	1.11	74.0	19.4	40.0	0.67	72.0	19.3	15.8	0.64	71.0	7.2	26.6	2022	[77]
18.5	1.17	81.1	17.7	38.6	0.66	70.3	18	15.5	0.65	73.7	7.4	25.1	2022	[91]
23.71	1.26	84.78	25.41	19.34	0.59	82.76	20.25	–	–	–	–	34.88	2023	[92]
23.74	1.139	80.1	21.68[a]	38.61	0.74	81.0	22.99	17.12	0.72	80.0	9.82	31.5	2023	[93]
21.40	1.16	81.1	20.13	41.61	0.72	75.1	22.50	20.63	0.70	74.7	10.78	30.91	2023	[94]
24.0	1.131	84.2	22.6[a]	41.7	0.698	81.9	23.8	13.7	0.678	82.5	7.7	30.3	2023	[95]
20.29	1.217	77.56	19.15[a]	40.74	0.716	82.15	23.95	17.5	0.701	78.91	9.68	28.83	2023	[96]
18.43	1.26	76.36	17.76	42.88	0.67	77.90	22.53	17.78	0.65	77.98	9.00	26.76	2023	[97]
19.98	1.15	77.51	17.80	39.52	0.68	75.77	20.38	18.38	0.66	72.97	8.79	26.59	2023	[98]

[a] Certified power conversion efficiency.
[b] Aperture Area in cm^2.

hindered by the lack of surface texturing and passivation on the Si cell. 2-T tandem cell designs often use TCOs as recombination layers, but this can result in optical losses. These recombination interlayers play a crucial role in minimizing optical losses and enhancing charge extraction. Sahli et al. [99] exchanged the TCO layer with nanocrystalline Si, achieving a PCE of 18 % for cells having an active area of 12.96 cm^2. In addition, to reduce reflection loss, they created a fully textured 2-T TSC with a nanocrystalline Si recombination interlayer **(**Fig. 11**(a))** [100]. Combining thermal evaporation and solution processing, a conformal PVSK layer was created. The certified PCE was 25.2 %, with superb current matching at 20.1 and 20.3 mA/cm^2 for the top and rear cells, respectively, as confirmed in Fig. 11**(b).** Furthermore, nanocrystalline Si oxide (nc-SiOx:H) was proposed as an intermediate layer between Si and PVSK cells, reducing infrared reflection losses [101]. This led to a 1.4 mA/cm^2 current density gain in the Si rear-cell with a 110 nm thick interlayer. The stabilized PCE was 25.2 %, with a total J_{SC} of 38.7 mA/

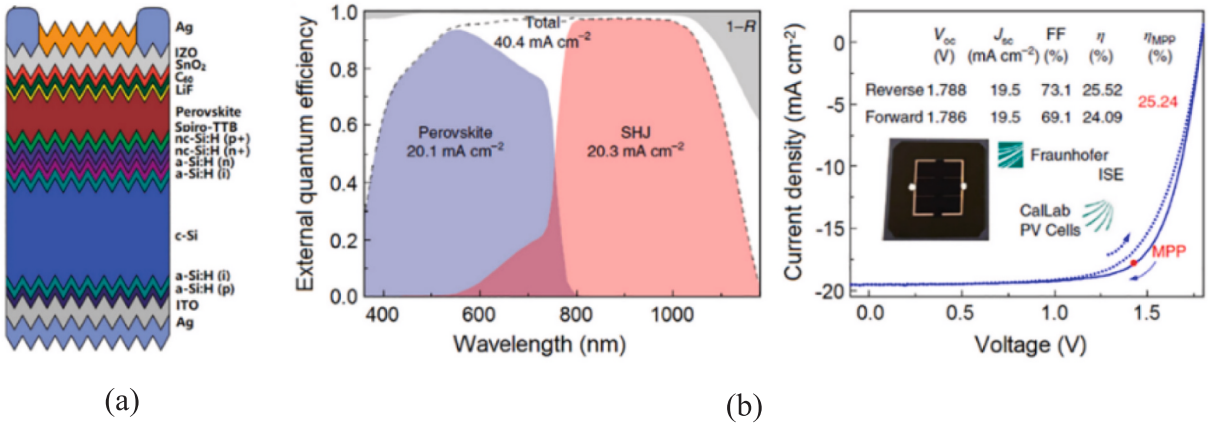

Fig. 11. (a) Entirely textured 2-T PVSK-Si TSC [100], (b) EQE curves of a current-matched fully textured 2T- PVSK/Si TSC with the J-V characteristic curves of the textured 2-T PVSK/Si TSC [100].

cm^2 under AM1.5G illumination (for the champion 1 cm^2 monolithic TSC).

4.2.2. Electron transport layer

The Si rear cell commonly uses a heterojunction configuration for better V_{OC}, ease of fabrication, and higher efficiency [102,103]. However, a key constraint is the thermal instability of a-Si:H, which cannot withstand temperatures above 200 °C, making it unsuitable for high-temperature sintered TiO_2 deposition. To overcome the thermal limitations of a-Si:H, an alternative approach, suggested by Albrecht et al. [104], involves a planar PVSK sub-cell with a compact ETL. The semi-transparent PVSK sub-cell was synthesized at 120 °C using atomic layer deposition (ALD) (Fig. 12) for SnO_2 and high-temperature mesoporous TiO_2. The multilayer transparent top contact consisted of sputtered ITO, spiro-OMeTAD, and MoO_3. The SnO_2 and ITO acted as the recombination layer, with a lithium fluoride (LiF) antireflective coating on the top contact. They successfully constructed a monolithic 2-T TSC with SHJ and PVSK, achieving a stabilized efficiency of 18.1 %. This approach ensures optimal temperature conditions and could be further enhanced with an organic polymeric thin film.

Recent studies have investigated various strategies for modifying ETLs and identifying potential ETL materials to improve charge extraction efficiency in PVSK-SCs. In this regard, reduced graphene oxide (rGO) has been incorporated into PCBM ETL of planer inverted PVSK-SCs by utilizing both the $CH_3NH_3PbI_{3-x}Cl_x$ PVSK deposited through a one-step methodology and the $CH_3NH_3PbI_3$ deposited through a two-step spin coating process. By increasing the PCBM conductivity with rGO as an additive, the J_{SC} and FF were enhanced, whereas the surface traps were decreased, leading to an increase in the V_{OC} and a hysteresis-free 14.5 % PVSK-solar cell [105]. Furthermore, Werner et al. [106] employed a PEIE/PCBM bilayer as dual ETLs to fabricate a planar semitransparent PVSK cell via low-temperature processing. The integrated low-temperature monolithic 2-T PVSK/SHJ tandem achieved a PCE of 21.2 % for 0.17 cm^2 and 19.2 % for an area of 1.22 cm^2, respectively with optimized HTL thickness.

4.2.3. Material properties and processing requirements

While SHJ cells offer high V_{OC} and efficiency, homojunction c-Si cells provide superior high-temperature tolerance, making them suitable for 2-T tandem integration. Wu et al. [107] introduced a 2-T TSC with homojunction c-Si as the back cell and mesoscopic PVSK as the front cell **(**Fig. 13**(a)).** The rear c-Si cell's enhanced temperature tolerance provides greater flexibility in PVSK-SC design and fabrication. Surface passivation and texturing led to 22.5 % steady-state efficiency after 1200 s of illumination and a V_{OC} of 1.75 V for a tandem with 1 cm^2. Zheng et al. [108] created a 2-T $MAPbI_3$/homojunction Si TSC without

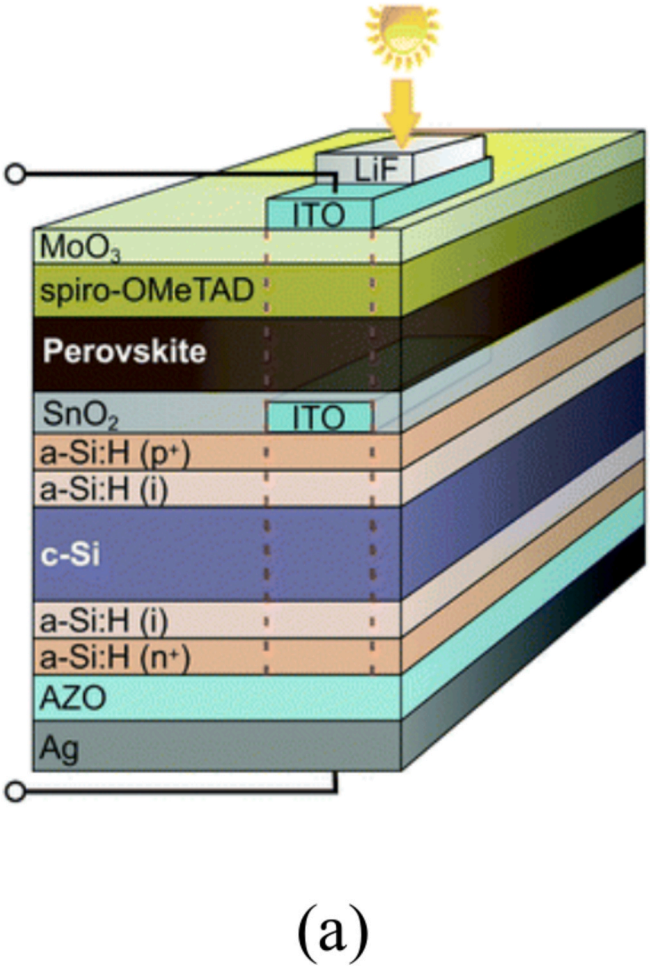

Fig. 12. 2-T PVSK/Si TSC with ALD deposited SnO_2 as the ETL [104].

an interface layer, using SnO_2 as an ETL and recombination interlayer. The champion cell accomplished a PCE of 21.0 % on 4 cm^2 with a V_{OC} of 1.67 V and PCE of 20.5 %. Shen et al. [109] developed interlayer-free 2-T tandems with ALD-TiO_2 as both the ETL and recombination interlayer, achieving PCEs of 24.1 % and 22.9 % for passivating contact heterojunction and homojunction tandems, respectively.

Most high-performance PVSK/Si tandem devices use an n-type SHJ rear cell. However, Nogay et al. [110] presented a 2-T TSC with a p-type

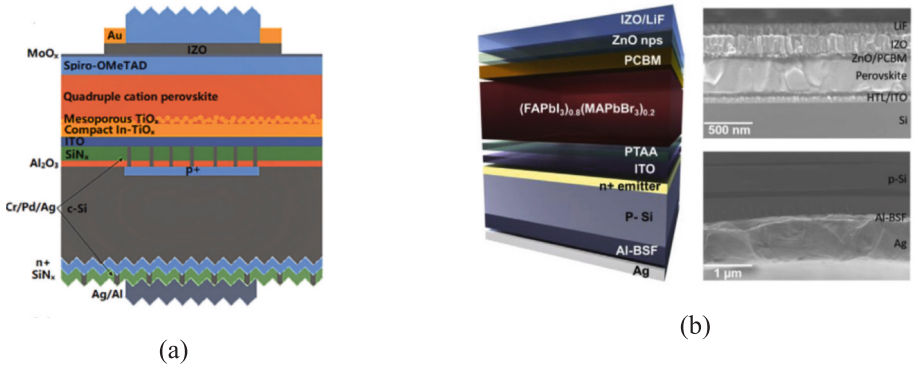

Fig. 13. (a) PVSK/Si TSC using homojunction Si [107], (b) Schematic and SEM of a monolithic PVSK/Si TSC (Ag/Al back-field (Al-BSF)/p– -Si/ n + -Si/ITO/PTAA/$(FAPbI_3)_{0.8}(MAPbBr_3)_{0.2}$/PCBM/ZnO/IZO/lLiF) [111].

wafer, achieving an efficiency of 25.1 %. This approach required an annealing temperature above 800 °C to create a passivation layer and reduce contact resistivity and parasitic absorption. Also, Kim et al. [111] fabricated a 2-T PVSK/Si TSC with a p-type Si rear cell. They determined that a 310 nm PVSK layer was ideal for achieving perfect current matching. Experimenting HTLs like PEDOT:PSS, PTAA, and NiO_x to reduce V_{OC} losses, they optimized the device with PTAA as the HTL, as realized from Fig. 13**(b)**, causing a V_{OC} of 1.645 V and peak PCE of 21.19 %. This was higher than the individual PVSK (13.4 %) and Si (12.8 %) sub-cells, with a J_{SC} rise from 14.91 mA/cm^2 to 16.12 mA/cm^2 due to heightened light absorption by the Si rear cell.

4.2.4. *Optical Enhancement in PVSK-SCs*

To further improve TSC performance, the optoelectronic properties of ETLs and the PVSK absorber's optical density must be considered. Qiu et al. [112] compared four PVSK materials to optimize 2-T PVSK/Si tandem cells **(**Fig. 14**(a)).** They adjusted the PVSK absorber's band gap and thickness to accomplish current matching between the corresponding cells **(**Fig. 14**(b)).** The PVSK film $FA_{0.5}MA_{0.38}Cs_{0.12}PbI_{2.04}Br_{0.96}$ (E_g = 1.69 eV) had a lower trap concentration of 1.13 × 10^{16} cm^{-3}, in comparison to $FA_{0.57}MA_{0.43}PbI_{2.04}Br_{0.96}$ (5.7 × 10^{16} cm^{-3}), with a similar band gap. The champion tandem device with $FA_{0.5}MA_{0.38}Cs_{0.12}PbI_{2.04}Br_{0.96}$ accomplished a J_{SC} of 16.5 mA/cm^2 and

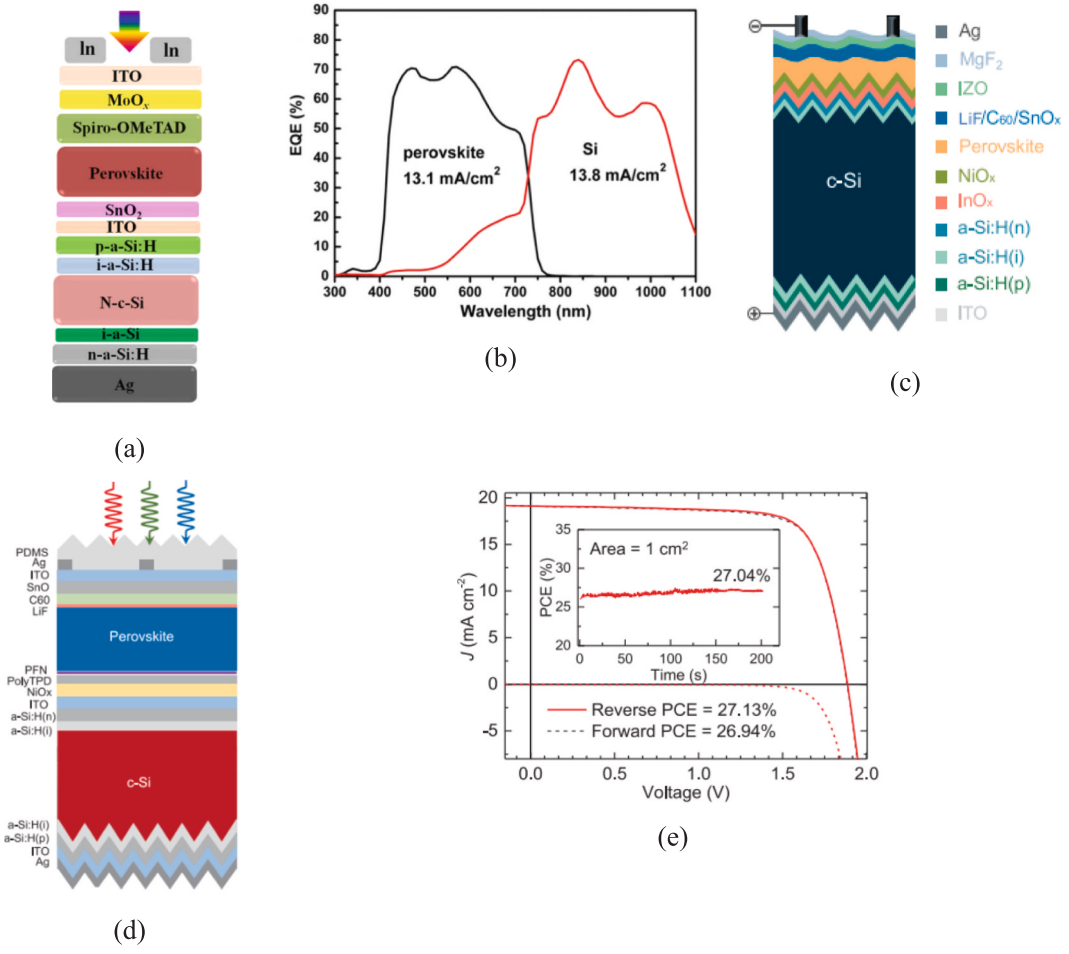

Fig. 14. (a) Schematic image of monolithic PVSK/Si TSC [112], (b) EQE of cells based on the 1.69 eV PVSK absorber [112], (c) Schematic of solution-processed PVSK–textured Si cell [116], (d) Schematic of the 2-T monolithic TSC [115], and (e) J-V characteristics of the champion TSC [115].

an efficiency of 22.22 %. The PCE output at 1.42 V, after 200 s of continuous illumination, exceeded 20.6 %.

Fine-tuning layers are crucial for improving optical performance [101,113]. To optimize efficiency, contact layers [114], perovskite composition [115], deposition [87], and additives must be optimized, as demonstrated by Chen et al. [55]. They used MACl and MAH_2PO_2 additives in the PVSK precursor, improving the grain morphology of WDB PVSK films and increasing photocurrent. MACl increased grain size, whereas MAH_2PO_2 reduced non-radiative recombination by passivating grain boundaries. By fine-tuning the top PVSK bandgap, they fabricated a TSC with a 1.64-eV WBG PSVK-SC on a rear SHJ cell, achieving a high overall TSC V_{OC} of 1.80 V and an efficiency of 25.4 %. Solution-processed PVSKs have enabled single-junction PCEs exceeding 20 %. Hou et al. [116] demonstrated a 2-T TSC linking a solution-processed micrometer-thick PVSK-SC with a textured SHJ cell **(**Fig. 14**(c)).**

In the 2-T design, cell efficiency is restricted by the bottom sub-cell. Enhancing its infrared sensitivity could improve overall performance. SHJ solar cells, with efficiencies around 26 %, high V_{OC}, and low-temperature manufacturing, have gained significant attention [117–119]. Tandem devices using top-side flat Si wafers, while potentially inferior optically compared to textured wafers, hold great promise for PCE because of their compatibility with solution processing and minimal adjustments to perovskite processing conditions. Deniz et al. [120] introduced two key advancements to enhance PCE in tandem devices with spin-coated PVSK layers on top-side flat Si wafers. First, the phosphonic acid-based additive pFBPA in the PVSK precursor removed lead-related defects and reduced non-radiative recombination at the PVSK/C_{60} interface, improving FF and V_{OC}. Second, SiO_2 nanoparticles were used as an interlayer beneath the PVSK film to reduce pinholes and shunts caused by pFBPA, while improving surface wettability for Me-4PACz as an HTL. Combining these advancements, the TSC device accomplished a conversion efficiency of 30 ± 1 % and a peak of 30.9 % for a 1.17 cm^2 active area. The device's operational stability was tested under 1-sun light illumination without encapsulation, retaining 85 % to 95 % of its peak PCE after 84 h of testing.

Finally, adjusting the perovskite bandgap and optimizing interface layers are essential strategies for enhancing light absorption and stability. Xu et al. [115] applied triple-halide alloys (Cl, Br, I) to adjust bandgap energy and stabilize the cell during light exposure. By replacing I with Br, they improved carrier lifetime and mobility in a 1.67 eV WBG p-i-n heterostructure top PVSK-SC. Incorporating an NiO_x layer (20 nm) between the ITO and HTL interface, as seen in Fig. 14**(d)** lowered shunting and enhanced yield in the 1 cm^2 TSC compared to poly-TPD-only HTLs. The stabilized PCE of the 1 cm^2 2T multijunction was 27.04 % with a V_{OC} of 1.886 V, as shown in Fig. 14**(e).** Kim et al. [121] showed a stable and efficient PVSK/Si TSC by incorporating phenethylammonium (PEA)-based two-dimensional additive ($I_{0.25}SCN_{0.75}$) into the PVSK precursor. SCN^- promoted grain growth, leading to a PVSK-SC with a WBG of 1.68 eV and an efficiency of 20.7 %. The PEA ($I_{0.25}SCN_{0.75}$) additive formed a 2D lead iodide framework at the surface

Table 4
Summary of Two-terminal configuration PVSK/Si based TSCs progress in recent years.

Top cell				Bottom cell				2-T TSC					
J_{sc} (mA/cm^2)	V_{oc} (V)	FF (%)	PCE (%)	J_{sc} (mA/cm^2)	V_{oc} (V)	FF (%)	PCE (%)	J_{sc} (mA/cm^2)	V_{oc} (V)	FF (%)	PCE (%)	year	Ref.
18.7	0.98	78.8	14.5	–	–	–	–	18.1	1.65	79.0	23.6	2017	[122]
13.7	1.583	75.0	16.3	22.45	0.634	78.0	11.1	16.1	1.676	78.0	21.0/20.5[a]	2018	[108]
–	–	–	–	–	–	–	–	16.2	1.74	78.0	21.9/21.8[a]	2018	[123]
21.5	1.16	76.0	18.9	36.2	0.665	72.7	17.5	17.8	1.763	78.1	24.5/24.1[a]	2018	[109]
19.6	1.05	77.0	15.8	–	–	–	–	18.4	1.77	77.0	25.0	2018	[124]
17.94	1.019	75.3	13.75	31.8	0.693	76.6	16.45	16.8	1.751	77.5	22.8/22.0[a]	2018	[99]
16.7	1.039	65.6	11.35	39.1	0.723	79.7	22.57	19.5	1.788	73.1	25.52/25.24[a]	2018	[100]
16.17	1.162	69.64	13.09	41.44	0.641	67.85	18.03	16.5	1.655	81.1	22.22	2018	[112]
21.6	1.1	77.9	18.4	35.7	0.7191	79.7	20.5	19.02	1.7919	74.60	25.43/25.2[a]	2019	[101]
–	–	–	–	–	–	–	22.6	19.5	1.741	74.7	25.41/25.1[a]	2019	[110]
15.96	1.13	74.57	13.45	28.56	0.575	78.06	12.82	16.12	1.645	79.92	21.19	2019	[111]
20.9	1.15	80.4	19.3	–	–	–	–	17.8	1.8	79.4	25.4	2019	[55]
19.3	1.16	79.1	17.7	–	–	–	–	19.2	1.82	75.3	26.2	2020	[125]
19.3	1.214	80.2	18.59/18.52[a]	–	–	–	–	19.12	1.886	57.3	27.13/27.04[a]	2020	[115]
–	–	–	20.7	35.11	0.644	76.0	17.28	19.2	1.756	79.2	26.7	2020	[121]
20.3	1.15	84.0	20.0	36.16	0.729	78.3	20.66	19.26	1.90	79.52	29.05/29.15[a]	2020	[114]
25.7	1.05	75.91	20.4	–	–	–	–	18.57	1.69	78.87	24.72/24.58[a]	2021	[126]
22.1	1.22	76.0	20.5	35.4	0.711	75.5	19.0	19.6	1.84	76.0	27.4	2021	[127]
23.2	1.13	78.1	20.4	36.5	0.713	77.5	20.2	19.2	1.78	76.8	26.2	2021	[128]
19.78	–	–	–	–	–	–	–	19.3	1.85	80.1	28.7	2022	[129]
20.31	–	–	–	19.7	–	–	–	19.48	1.92	79.4	29.75/29.8[a]	2022	[130]
23.74	1.139	80.1	21.68[a]	38.61	0.74	81.0	22.99	18.81	1.79	78.0	26.34[a]	2023	[93]
–	–	–	–	–	–	–	–	20.87	2.09	82.0	35.9	2023	[131]
–	–	–	–	–	–	–	–	18.1	1.819	82.4	27.2/27.0[a]	2023	[132]
22.40	1.21	82.30	22.31	–	–	–	–	19.48	1.9	76.42	28.35	2023	[133]
22.9	1.17	81.3	21.8/21.0[a]	–	–	–	–	19.4	1.85	81.8	29.3/29.0[a]	2023	[134]
–	–	–	–	35.85	0.719	77.53	20.0	20.47	1.91	79.8	31.25	2023	[135]
–	–	–	–	35.5	0.672	79.7	19.0	19.7	1.83	81.0	29.2/28.76[a]	2023	[136]
20.5	1.26	82.6	21.3	–	–	–	–	19.1	1.91	79.1	28.9/29.0[a]	2023	[137]
20.9	1.207	80.8	20.3	38.8	0.714	77.7	21.5	20.1	1.849	77.6	28.8/28.3[a]	2023	[138]
–	–	–	–	–	–	–	–	19.812 ± 0.86 %	1.9528 ± 0.48 %	79.9 ± 1.07 %	30.93 ± 30.9[a]	2024	[120]
22.27	1.15	85.48	22.74/21.2[a]	–	–	–	–	20.01	1.81	82.91	30.05	2024	[139]

[b] Aperture Area in cm^2.
[a] Certified power conversion efficiency.

and grain boundaries, enhancing passivation. The champion monolithic tandem accomplished a PCE of 26.7 %. Al-Ashouri et al. [114] developed a 2-T TSC with a $Cs_{0.05}(FA_{0.77}MA_{0.23})_{0.95}Pb(I_{0.77}Br_{0.23})_3$ PVSK absorber ($E_g = 1.68$ eV) and a 260-μm-thick n-type SHJ cell. A certified efficiency of 29.15 % was achieved at the 1 cm^2 device scale, with an FF of 77.8 % and a V_{OC} of 1.897 V. The progress of 2-T PVSK/Si TSC devices is listed in Table 4.

5. Challenges and future prospects

PVSK-SCs continue to be investigated with respect to their sustainability and scalability. Performance parameters are enhanced by integrating PVSK-SCs with other advanced PV technologies. Perovskite-based TSCs exhibit significant potential in terms of their efficiency, which is a highly promising advancement. In light of the demonstrated validity of Si PV cells in the present market, the metrics that enable a soft transition from laboratory investigations to industrial-scale manufacture are of considerable attention.

The top PVSK-SC must meet the same field confidence guidelines as the rear Si cell in order to be commercially viable in a Si-based TSC panel. Additionally, wafers intended for industrial manufacturing should be employed to fabricate TSCs, and only materials and technologies that are of minimal cost must be employed. One of the numerous challenges to commercializing this technology is the scaling up of cells to module size. Additionally, the operating lifetime that extended to twenty-five years is another significant obstacle. Also, additional processing and design challenges summarized in Fig. 15 must be considered to achieve current matching at the highest photocurrents. To address these concerns, it is imperative to thoroughly consider the following strategies and obstacles for future advancements.

5.1. Comparison between PVSK/Si and other candidates

Perovskite/silicon TSCs represent a significant advancement in PV technology, distinguished by their remarkable efficiency and stability compared to perovskite/CIGS tandems. As of December 2021, perovskite/Si tandems achieved a record PCE of 29.8 %, leveraging the established performance of Si alongside the high absorption capabilities of PVSK materials [140]. On the other hand, perovskite/CIGS tandems generally show lower efficiencies (typically below 26 %) [141]. The notable superiority of perovskite/Si TSCs extends beyond mere efficiency; they exhibit enhanced stability against environmental degradation, outperforming CIGS cells in tests involving moisture, UV exposure, and thermal conditions. Innovative architectural designs, including inverted structures that protect sensitive materials, have contributed to this durability, further establishing perovskite Si tandems as a viable long-term energy solution. [140]. In contrast, CIGS cells face inherent material limitations and more complex production processes that hinder their commercial viability and overall performance [140].

Furthermore, Si solar cells are the industry standard, making perovskite/Si tandems easier to integrate into existing manufacturing lines. Silicon wafer production is highly mature, with low-cost fabrication and well-established infrastructure. CIGS technology, while promising, has a smaller market share and less developed large-scale production capabilities. In addition, cost-effectiveness is another area where perovskite/Si tandem technology shines. The ongoing development of low-cost manufacturing methods, such as inkjet printing and roll-to-roll processing, positions these cells favorably within a

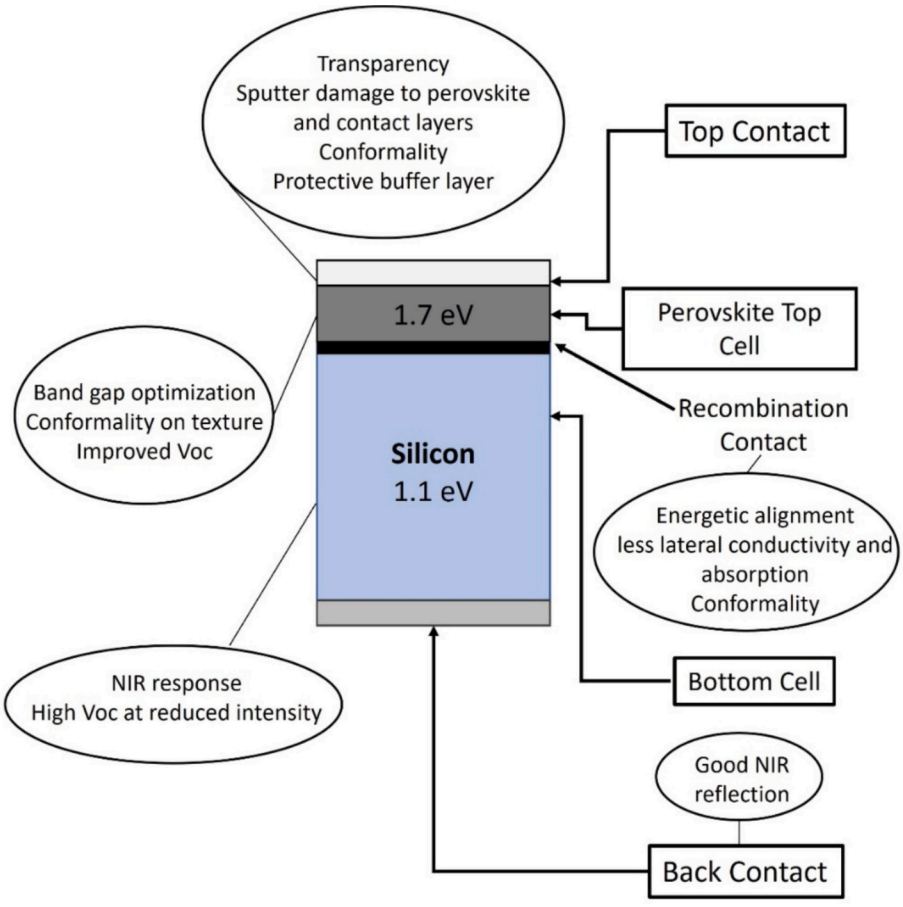

Fig. 15. Engineering and scientific challenges for advancing each tandem architecture, along with a schematic representation of monolithic perovskite TSCs featuring silicon-based bottom cell.

competitive market, potentially reducing production costs below €0.40/Wp [140]. Despite their advantages, the adoption of perovskite/Si tandems is not without challenges. Issues such as the long-term stability of perovskite materials, regulatory scrutiny concerning sustainability, and the need for responsible material sourcing remain critical considerations for future development and market acceptance [142]. Nevertheless, as the urgency for efficient and sustainable energy sources escalates, PVSK/Si tandem solar cells are poised to show a pivotal role in the evolution of renewable energy technologies, aligning both corporate sustainability goals and regulatory frameworks aimed at reducing carbon emissions [142,143]. Apart from this, there is a significant amount of research and development focused on PVSK/Si tandem cells, driven by the potential for high efficiencies and the compatibility with existing silicon technology. This has led to rapid advancements in this area. While there is research on perovskite/CIGS tandems, it is less extensive compared to PVSK/Si, partly due to the lower efficiency potential and higher complexity.

5.2. Device structure

Although both sub-cells are unrelated, electrically, in 4-T tandems, the device can remain to function, albeit with a reduced power, if one of the sub-cells is not operational or malfunctioning. While the collapse of one sub-cell or the recombination interlayer in 2-T tandems configuration will result in the destruction of all devices, as both sub-cells are directly coupled. The enhancement of high-performance semi-transparent front PVSK-SCs is a critical challenge for the four terminal tandem devices. In the interim, it is imperative to consider the optimization of transparent electrodes to minimize parasitic absorption and the incorporation of appropriate ARC layers to reduce reflection. In contrast to 2-T structures, 4-T tandems are susceptible to parasitic absorption and reflection due to the existence of supplementary transparent contacts and interfaces, which could eventually reduce their efficacy. This explains why the majority of TSCs discussed in literature are in two terminal topologies. It is anticipated that the 2-T architecture will continue to be the dominant trend in the future. In addition to optimizing each sub-cell, decent current matching between both sub-cells and minimal energy loss are essential for constructing and developing effective 2-T tandem devices. Therefore, the interfaces and the bandgap of the perovskite that is in accordance with the current produced by each sub-cell should be optimized.

It is approved theoretically that Si is deemed to have an optimal E_g of 1.73 eV for the front cell. However, considering a front E_g of 1.65 to 1.85 eV, it is still theoretically possible to achieve higher efficiencies above 40 % [71,144]. From a practical point of view, even with the optimum E_g is met, optimizing high-quality Si with a 2-T tandem connection is a daunting task. Producing efficiencies that surpass that of the single junction Si cells has been a difficult task due to the absence of promptly available, exceedingly efficient WBG top cells (beyond the III–V growth). Additionally, the recombination interlayers in 2-T TSCs should effectively avoid halide ion migration. Notably, Si surfaces are notoriously sensitive to impurities and may be poisoned by halide ions. Another substantial obstacle to the efficient design and optimization of TSCs is the guarantee of process compatibility during the multilayer fabrication process. The maximal processing temperature of the top sub-cell must be able to withstand the back sub-cell and p-n junction of a substrate device, while the reverse is true for a superstrate cell. By connecting two completely functional devices, it is possible to decouple the challenges correlated with temperature compatibility [6,71].

5.3. Lead toxicity and related environmental issues

The acceptance and adoption of new technologies are significantly influenced by the environmental and public health consequences [145]. When contemplating commercialization. lead toxicity because of the existence of Pb in the absorber layer of PVSK for Pb-based based TSCs is a significant cause for worry. When perovskite, for example, $MAPbI_3$, is exposed to water, it rapidly decomposes into MAI and PbI_2 [146,147]. The relatively high solubility of PbI_2 in water increases the probability of Pb being released into the atmosphere in the occurrence of disastrous events such as fire or flooding [147]. Neurological disorders can be caused by Pb exposure in humans, animals, and plants [148]. Protective measures must be implemented throughout the non-vacuum deposition of PSVK-SCs in TSCs to prevent Pb release in the fabrication process of PSVK-SCs. In order to mitigate the environmental and human consequences of lead, it is necessary to implement solution recycling methods. In comparison to non-vacuum deposition processes, the vacuum deposition of PSVK-SCs conclusively reduces Pb hazards because of the removal of chemical solutions, restraining Pb. Further, the vacuum deposition technique prevents the liberation of Pb into the environment. Strategies for addressing environmental issues related to Pb can be derived from CdTe industrial lines [149].

Encapsulation is a viable approach that can effectively mitigate the issue of lead leakage. If suitable encapsulation is implemented, the PVSK tandems can be utilized with minimal lead leakage. As previously reported, the lead leakage rate is lowered by a factor of 375 when using an epoxy resin, as opposed to the encapsulation procedure that involves a glass cover with a UV-cured resin at module edges [150]. It is encouraging to note that a variety of encapsulating materials and methodologies have been engineered for PVSK-SCs, which significantly reduce the potential for Pb-leakage [151,152]. The effect of Pb on the atmosphere and humans can be completely eliminated by replacing Pb-free perovskites with Pb-based perovskites. This is an additional approach to resolving the environmental issue associated with lead. Numerous research groups are engaged in the development of lead-free PVSK-SCs that contain Sn, Ag, Sb, Br, and other elements [153–157]. Sn-based PVSK-SCs demonstrate the utmost efficiency among them. Despite the abundant attempts to boost the PCE of Sn-based PVSK-SCs, the PCE remains considerably inferior to that of Pb-based cells [158]. This is primarily on account of the straightforward oxidation of Sn^{2+} to Sn^{4+} so it is imperative to create Sn-based PVSK-SCs that are highly efficient by moderating crystallization and diminishing Sn^{2+} oxidation.

Recycling PVSK-based tandem modules is another encouraging approach to mitigate the negative impacts of Pb on the environment and human health. Developing an efficient encapsulation technique that effectively prevents any harmful substances from PVSK-SCs from flowing into the environment is essential for the commercialization of Pb-based PVSK. Prior to the commercialization of PVSK-SCs, defining and implementing reliable processes for module recycling after the PVSK-SCs are decommissioned is crucial. In the future, it is necessary to stem more advanced encapsulation techniques and conduct extensive outdoor experiments to evaluate their effectiveness in reducing Pb leakage. Furthermore, additional life cycle assessments (LCAs) and real field evaluations are still necessary before any definitive conclusions regarding the impact of Pb on the environment, particularly in the context of PVSK-based TSCs, can be reached. Finally, it is also crucial to integrate theoretical calculations and experiments in order to investigate innovative, environmentally favorable, and energy-efficient photovoltaic devices.

5.4. Scalability of PVSK-based TSCs

For the industrialization of PVSK-based TSCs, high-PCE large-scale tandem modules fabrication utilizing perovskite layers with good homogeneity is an essential technology. At present, the majority of high-performance PVSK-based TSCs and PSVK-SCs are yet at the lab cell level, with active areas that are less than 1 cm^2. The decline in PCE as module size increases has been identified as a key factor to deliberate when assessing the scalability of PV technology [159]. The large-scale fabrication of PVSK-based tandems in conjunction with develop industry modules is primarily dependent on the improvement of equipment and fabrication processes for homogeneous PVSK layers and other

thin films in PVSK modules, specifically on textured Si modules, through blade coating or vacuum deposition procedures to achieve conformal coating of PVSK-SCs on an industrial level [160].

One of the challenges is making PVSK that is free of any pinholes and has a low defect density that fits perfectly on Si. To boost the performance of TSC modules, it is imperative to implement CTLs and transparent contacts having high transmittance, as well as to incorporate appropriate ARC layers to further mitigate optical losses. Creating tunnel junctions or recombination layers using a solution-based approach on rough surfaces poses a greater difficulty compared to producing perovskite thin films, mostly due to their reduced thickness. Also, on an industrial scale, the production of uniformly thick perovskite films of exceptional quality necessitates rigorous process control and solution quality via solution-processing methods [161].

To prevent processing impairment in the bottom cell, it is crucial to carefully select the solvents used in these operations. By employing vapor-processing techniques, these challenges can be avoided. The vapor-based processing strategy is a widely recognized practice in the PV industry [162] and offers a variety of advantages, such as the ability to develop a compact and even film over a vast area, the ability to manage the thickness, the ease of deposition on a coarse substrate, the aptitude to process without solvents, and the capability to operate at a reduced temperature. Thus, it is an exceptional option for the development of tandem modules that are perovskite-based. The vapor deposition method was employed by Oxford PV company to fabricate 2-T PVSK/Si tandems with a champion efficiency of 28 % on a large scale [163]. The simplicity of fabricating conformal films and the comparatively high manufacture cost of vacuum deposition methodologies should be taken into consideration in comparison to solution methods. Vacuum deposition methods continue to pose a challenge in the production of perovskites with complex compositions and optimal band gaps, and the uniformity of composition must be precisely controlled. Nevertheless, the large-scale fabrication of PVSK/QD, PVSK/DSSC, and all-PVSK-TSCs is contingent upon the perovskite modules and other layers in all subcells. Metal and TCO layers are included in the transparent electrodes of PVSK-based TSCs. Thermal evaporation is used to deposit the ultra-thin Ag, Au, and Cu layers, which can be used to create semitransparent PVSK-SCs [58,59,61]. In addition, these metal layers are employed as recombination layers in the majority of 2-T PVSK/Organic tandem cells [164–166]. An essential concern for perovskite TSCs is the deposition of TCOs in the upper cells, RLs, and subcells without causing damage to the existing subcells beneath. In addition to sputtering and plasma enhanced chemical vapor deposition methods, rapid plasma deposition is highly promising for the preparation of TCOs for both semitransparent PVSK-SCs and recombination layers. Strategies to prevent the destruction of preexisting sub-cells in tandem configurations include the use of innovative, environmentally friendly orthogonal solvent systems, the application of a solvent-free methodology to deposit the second sub-cell, and the innovation of a barrier layer that is sufficiently effective [167]. Sputtering is a common method for depositing TCOs, including ITO and IZO, which can serve as recombination interlayers in 2-T PVSK/Si and PVSK/CIGS TSCs [89,106–109,122–124,141,168–171].

In order to safeguard the CTLs and PVSK from damage during sputtering, buffer layers are frequently used when they are employed as transparent contacts in PVSK cells. In general, these buffers consist of thermally deposited MoO_3 layers or ALD-deposited AZO and SnO_2 films [62,122]. Traditional TCO recombination layers in large area 2-T PVSK/Si tandems exhibit high lateral conductivity, which leads to shunt paths through pinholes and defects of the PVSK-SC. The TCO recombination interlayers are to be replaced with high-shunt-resistance materials [99–101] may serve as an efficacious solution. In previous research, solution-processed organic materials have been employed as recombination interlayers in 2-T all-PVSK and PVSK/Organic TSCs. It is also essential for large-scale fabrication to optimize interconnection design to obtain a competent assessment between resistive losses, leakage current paths, and losses from dead areas.

The development of high-quality PVSK layers with large areas is central to producing highly efficient large-area TSCs. Slot-die coating and roll-to-roll printing, blade coating, and inkjet printing are fabrication techniques that are used to create PVSK solar cell modules, and they have the prospect of being used in large-area PVSK-based TSCs and require further progress [160]. Furthermore, thermal evaporation may also be a viable option for the deposition of high-quality perovskite films. The development of high-performance flexible tandem devices is an optimistic direction, as PVSK, CIGS, and organic PV cells can be manufactured on flexible substrates. Also, a prospective and viable strategy for reducing material costs and concurrently reducing electronic and optical losses is the fabrication of large-scale TSCs that are free of recombination layers or tunnel junctions.

In conjunction with efficiency development, efficient approaches for significantly reducing the levelized cost of electricity of PVSK-based tandems include the development of Indium-free TCOs and recombination interlayers, equipment cost reduction, capacity enhancement, and repeatability improvement as it is the primary problem to their commercialization. Presently, government and industrial financial support are currently instrumental in the commercialization of perovskite TSCs.

5.5. Long term stability

In contrast to well-established solar mechanisms such as Si-based and some TFSC technologies, including CdTe, which have exhibited exceptional endurance following a quarter century of field exposure and practical application, PVSK-based tandems, in general, encounter difficulties in satisfying the same durability parameters [53,172,173]. Stability has been a challenge for PVSK-SCs since their inception. The commercialization of PVSK-SCs has been hindered by instability issues of PVSK material has raised significant skepticism about promising technology. Regarding PVSK-based tandems, the primary cause of stability problems is the degradation of the most prevalent $MAPbI_3$ absorber upon exposure to water, oxygen, its poor ability to tolerate heat, moisture, and light because of its soft-matter nature [174]. The intrinsic instability of these crystals may be attributed to ion diffusion and migration and to the presence of organic components in the crystal lattice [175–177]. Ion migration is an inherent characteristic of perovskite materials, as they are ionic conductors and possess weak crystal structures, as well as the existence of vacancies and other defects.

Fig. 16**(a)** demonstrates the ion migration process in organometal halide PVSKs [178]. This behavior was initially identified by **Mizusaki et al**. in 1983 [179]. The authors hypothesized that ionic conduction in halide PVSKs was the result of the transfer of halide-ion vacancies within the PVSK lattice. Upon the occurrence of ion migration, the PVSK film composition and morphology may be altered because of the accelerated loss of PVSK ions under light illumination [180–182]. Perovskite films are susceptible to phase segregation, interfacial interactions, and undesirable band bending because of ion migration during device operation. The possibility to impede the passage of ions exists due to the passivation of defects. The hysteresis and instability of PVSK-SCs would be the consequence of ion movement within PVSKs when they are exposed to an electric field [183,184]. Notably, hysteresis is also perceived as a hindrance to developing robust PVSK-SCs. **Snaith et al.** [185] were the first to describe the J–V hysteric properties of PVSK-SCs. Hysteresis is the term used to describe the deviation in the J–V curves of the forward and reversed scans. During the reverse scan, the photocurrent decreases before attaining a steady state value. The opposite is true for the forward scan. Hysteresis is a significant factor because it is associated with the performance metrics and durability of PVSK-SCs over time. The hysteresis effects caused by various factors, like scan rate, PVSK composition, particle size, and device configuration, have been shown to influence PVSK-SCs in numerous studies [22,186–190]. In addition, **McGehee et al.** discovered that the hysteresis in PVSK cells

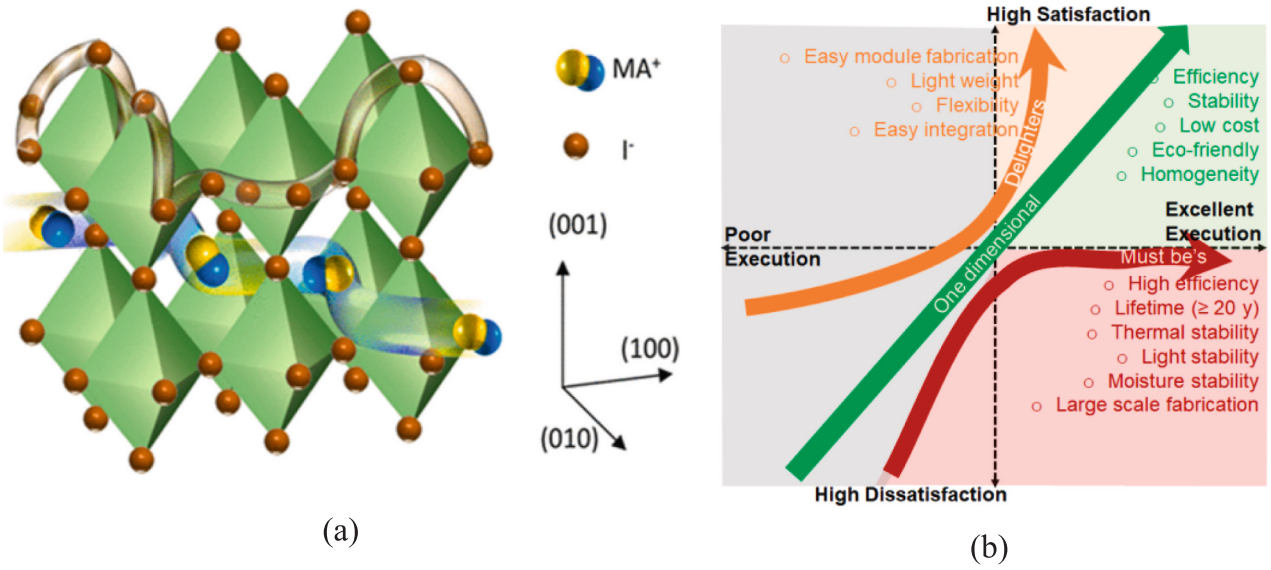

Fig. 16. (a) Diagram depicting ion migration within the perovskite lattice [178], (b) Kano model for proposing the successful commercialization strategy of PVSK-SCs [215].

was highly responsive to J–V measurement factors, including pre-bias, scan rate, and scan direction [191].

Furthermore, normal thermal instability is typically triggered by the loss of organic components (MA^+), which leads to numerous defects at the grain boundaries [192]. The passivation of grain boundary defects and the optimization of the "A" cation with proper materials are desirable solutions to this issue. To improve the thermal stability of PVSK films, numerous studies have concentrated on incorporating Cs^+ [76,193,194]. Usually, the addition of Cs can partly substitute the volatile A-site organic cations (i.e., MA^+, FA^+) with stable WBG PVSKs [193,195]. The stability of materials was significantly enhanced utilizing inorganic cations, including cesium, potassium, and, successively, rubidium that could maintain up to 95 % of their initial efficiency after operation at MPP for several hours [75,193,196–200]. The thermal stability of inorganic PVSK has been shown to be preferable to that of organic perovskite in numerous studies [165,197,200–202].

The intrinsic resistance of hybrid PVSKs to water, heat, light, and oxygen poses a significant challenge for PVSK-based TSCs at the material level. Preparing high-quality PVSK films with fewer defects and grain boundaries is the most fundamental method of enhancing device stability, thereby reducing water and oxygen destruction. It has been shown that the processes of passivating grain boundaries and surfaces and enhancing crystallinity and grain size of PVSK films are effective in suppressing halide segregation and enhancing long-term stability [73,203–205]. $CsPbI_3$ perovskite is an optimal top sub-cell material for TSCs due to its 1.73 eV bandgap [206–208]. Nevertheless, the primary obstacle is the phase stability. The total PCE of $CsPbI_3$ solar cells is nonetheless poorer than that of hybrid PVSKs with the same E_g, despite their potential value for tandem structures. The $CsPbI_3$ perovskite would be able to effectively participate in TSCs by enhancing its phase stability [206,207,209,210].

Besides the deterioration of PVSK films, the stability of the CTLs is additionally essential. It has been reported that dopants, including Li-TFSI, in the HTLs of spiro-OMeTAD and PTAA have the potential to damage PVSK films [211]. The development of novel dopant-free HTLs with raised mobilities has emerged as a research focus. Furthermore, the degradation of devices can be induced by the reaction between halides in perovskites and metal layers (Au, Ag, Al) [212,213]. In order to prevent these detrimental interactions, it may be beneficial to incorporate buffer layers or employ electrodes that are chemically stable. For tandem devices in general, encapsulation is an effective method to prevent the leakage of water-soluble toxic Pb compounds, as well as water and oxygen permeation. Concurrently, it is imperative to establish standardized stability tests, such as thermal stability, air stability, and photostability, to guarantee that the solar cells can withstand the outdoor environments for an extended period. As mixed-halide hybrid PVSKs are the primary photoactive material in most high-efficiency 2-T PVSK/Si tandems [214], PVSK-based TSCs will be prepared for commercialization once the stability of PVSK-SCs and encapsulation can be successfully resolved because solar cells must operate in light conditions that are sustained for extended periods.

Apart from this, the stability data presented by different researchers cannot be accurately compared due to the fact that the testing conditions used in each experiment, including humidity, temperature, and encapsulation technique, are varied. Remarkably, efficiency is a well-defined factor that can be justified in compliance with existing standards, while stability-related characteristics such as lifetime and deterioration rates are not. Consequently, it is imperative to establish a standardized test condition for the stability testing of PVSK cells, with a particular stress on the stability of the device under hysteresis, thermal stability, mechanical stability, and stability in light illumination, along with the presence of moisture and oxygen, regarding different fabrication processes. The Kano model, as seen in Fig. 16**(b)**, is a valuable resource for comprehending the prioritization of the features of PVSK-SCs in order to meet the current market demand and achieve effective commercialization [215].

6. Conclusions

This review summarizes the advancements of PVSK/Si TSCs. The discussion included a variety of TSC categories and their subsequent mechanisms, including the 2-T monolithic and 4-T stacked arrangements. PVSK/Si tandem cells have garnered the most attention among these devices as a result of their advanced fabrication technology and exceptional performance. It is likely that PVSK/Si tandem devices will be at the forefront of this field for a period of time. It is foreseeable that PVSK-based TSCs will become a research frontier, garnering an increasing number of interests. Performance enhancement, the intrinsic instability of perovskite materials, fabrication costs, lead toxicity, and scaling-up manufacturing are among the numerous critical obstacles that continue to impede the advancement of tandem devices. More commercialization-related issues will emerge as the conversion efficiencies for these PVSK-based TSCs are anticipated to continue increasing in the near future. It is imperative to enhance the testing and

evaluation systems for devices. Additionally, the long-term stability of TSCs must be taken into account to survive in severe environments, such as the ocean, desert, or space. Therefore, the development of TSCs through commercialization will be significantly influenced by the use of appropriate packaging, as well as high-efficient materials and PV cell manufacturing. Consequently, it is imperative to conduct interdisciplinary research to address a variety of obstacles in the commercialization of TSCs based perovskite materials in order to achieve positive results. PVSK-based tandem device technology offers a vast amount of space and an enormous number of prospects for the development of high-performance PV cells.

We are confident that the performance of PVSK-based TSCs will continue to astound us, specifically PVSK/Si tandems, given the significant and rapid advances that have been made in recent years. This will be accomplished via collaborative efforts involving device engineering and interface enhancements, advancements in material and cell stability, and the improvement of large-scale manufacturing technologies.

CRediT authorship contribution statement

Doaa Khodair: Writing – review & editing, Writing – original draft, Resources, Methodology, Investigation. **Ahmed Saeed:** Writing – review & editing, Writing – original draft, Visualization, Supervision, Resources, Investigation, Data curation, Conceptualization. **Ahmed Shaker:** Writing – review & editing, Writing – original draft, Visualization, Validation, Supervision, Resources, Methodology, Conceptualization. **Mohamed Abouelatta:** Writing – review & editing, Writing – original draft, Validation, Supervision, Resources, Methodology, Investigation, Conceptualization. **Omar A.M. Abdelraouf:** Writing – review & editing, Writing – original draft, Investigation. **S. EL-Rabaie:** Writing – review & editing, Supervision, Conceptualization.

Declaration of Competing Interest

The authors declare that they have no known competing financial interests or personal relationships that could have appeared to influence the work reported in this paper.

References

[1] K. ElKhamisy, H. Abdelhamid, E.S.M. El-Rabaie, et al., A comprehensive survey of silicon thin-film solar cell: challenges and novel trends, Plasmonics (2023), https://doi.org/10.1007/s11468-023-01905-x.

[2] J. Pastuszak, P. W˛egierek, Photovoltaic cell generations and current research directions for their development, Materials 15 (2022) 5542, https://doi.org/10.3390/ma15165542.

[3] C. Battaglia, A. Cuevas, S. De Wolf, High-efficiency crystalline silicon solar cells: Status and perspectives, Energy Environ. Sci. 9 (2016) 1552–1576.

[4] S. Maiti, M. van der Laan, D. Poonia, P. Schall, S. Kinge, L.D. Siebbeles, Emergence of new materials for exploiting highly efficient carrier multiplication in photovoltaics, Chem. Phys. Rev. 1 (2020) 011302.

[5] J.E. Jacak, W.A. Jacak, Routes for metallization of perovskite solar cells, Materials 15 (2022) 2254.

[6] M.T. Horantner, T. Leijtens, M.E. Ziffer, G.E. Eperon, M.G. Christoforo, M. D. McGehee, H.J. Snaith, The potential of multijunction perovskite solar cells, ACS EnergyLett. 2 (2017) 2506–2513.

[7] O.M. Saif, Y. Elogail, T.M. Abdolkader, A. Shaker, A. Zekry, M. Abouelatta, M. S. Salem, M. Fedawy, Comprehensive review on thin film homojunction solar cells: technologies, progress and challenges, Energies 16 (2023) 4402, https://doi.org/10.3390/en16114402.

[8] O.M. Saif, A.H. Zekry, M. Abouelatta, et al., A comprehensive review of tandem solar cells integrated on silicon substrate: III/V vs perovskite, SILICON 15 (2023) 6329–6347, https://doi.org/10.1007/s12633-023-02466-8.

[9] M. Anaya, G. Lozano, M.E. Calvo, H. Míguez, ABX_3 perovskites for tandem solar cells, Joule 1 (4) (2017) 769–793, https://doi.org/10.1016/j.joule.2017.09.017.

[10] P. Roy, A. Ghosh, F. Barclay, A. Khare, E. Cuce, Perovskite solar cells: a review of the recent advances, Coatings 12 (2022) 1089, https://doi.org/10.3390/coatings12081089.

[11] R. Wang, T. Huang, J. Xue, J. Tong, K. Zhu, Y. Yang, Prospects for metal halide perovskite-based tandem solar cells, Nat. Photon. 15 (6) (2021) 411–425, https://doi.org/10.1038/s41566-021-00809-8.

[12] H. Zhu, S. Teale, M.N. Lintangpradipto, et al., Long-term operating stability in perovskite photovoltaics, Nat. Rev. Mater. 8 (2023) 569–586, https://doi.org/10.1038/s41578-023-00582-w.

[13] RSC Adv., 2023, 13, 1787. (Stability of perovskite solar cells: issues and prospects).

[14] N.E.I. Boukortt, C. Triolo, S. Santangelo, S. Patanè, All-perovskite tandem solar cells: from certified 25% and beyond, Energies 16 (2023) 3519, https://doi.org/10.3390/en16083519.

[15] E.A.R. Assirey, Perovskite synthesis, properties and their related biochemical and industrial application, Saudi Pharm. J. 27 (2019) 817–829.

[16] N.-G. Park, Perovskite solar cells: an emerging photovoltaic technology, Mater. Today 18 (2) (2015) 65–72.

[17] C.J. Bartel, C. Sutton, B.R. Goldsmith, R. Ouyang, C.B. Musgrave, L. M. Ghiringhelli, M. Scheffler, New tolerance factor to predict the stability of perovskite oxides and halides, Sci. Adv. 5 (2019) eaav0693.

[18] W. Travis, E.N.K. Glover, H. Bronstein, D.O. Scanlon, R.G. Palgrave, On the application of the tolerance factor to inorganic and hybrid halide perovskites: a revised system, Chem. Sci. 7 (2016) 4548–4556.

[19] P. Kumar, S. Thokala, Surya Prakash Singh, Ranbir Singh, Research progress and challenges in extending the infra-red absorption of perovskite tandem solar cells, Nano Energy (2023), https://doi.org/10.1016/j.nanoen.2023.109175.

[20] A. Kojima, K. Teshima, Y. Shirai, T. Miyasaka, Organometal halide perovskites as visible-light sensitizers for photovoltaic, J. Chem. Soc. Chem. Commun. 131 (2009) 6050–6051.

[21] N. Jeon, J. Noh, Y. Kim, et al., Solvent engineering for high-performance inorganic–organic hybrid perovskite solar cells, Nature Mater 13 (2014) 897–903, https://doi.org/10.1038/nmat4014.

[22] N.J. Jeon, J.H. Noh, W.S. Yang, Y.C. Kim, S. Ryu, J. Seo, S. Seok, Il compositional engineering of perovskite materials for high-performance solar cells, Nature 517 (2015) 476–480.

[23] E.H. Jung, N.J. Jeon, E.Y. Park, et al., Efficient, stable and scalable perovskite solar cells using poly(3-hexylthiophene), Nature 567 (2019) 511–515, https://doi.org/10.1038/s41586-019-1036-3.

[24] Q. Jiang, Y. Zhao, X. Zhang, et al., Surface passivation of perovskite film for efficient solar cells, Nat. Photonics 13 (2019) 460–466, https://doi.org/10.1038/s41566-019-0398-2.

[25] J.J. Yoo, G. Seo, M.R. Chua, T.G. Park, Y. Lu, F. Rotermung, Y.K. Kim, C.S. Moon, N.J. Jeon, J.P. Correa-Baena, et al., Efficient perovskite solar cells via improved carrier management, Nature 590 (2021) 587–594.

[26] G. Kim, D.S. Kim, Development of perovskite solar cells with >25% conversion efficiency, Joule 5 (2021) 1033–1035.

[27] P.A. Ajibade, A.O. Adeloye, A.E. Oluwalana, M.A. Thamae, Organolead halide perovskites: Synthetic routes, structural features, and their potential in the development of photovoltaic, Nanotechnol. Rev. 12 (1) (2023) 20220547, https://doi.org/10.1515/ntrev-2022-0547.

[28] M. Mujahid, C. Chen, W. Hu, Z.-K. Wang, Y. Duan, Progress of high-throughput and low-cost flexible perovskite solar cells, Sol. RRL 4 (2020) 1900556.

[29] I. Hussain, H.P. Tran, J. Jaksik, J. Moore, N. Islam, M.J. Uddin, Functional materials, device architecture, and flexibility of perovskite solar cell, Emergent Mater. 1 (2018) 133–154.

[30] S. Nair, J.V. Gohel, A review on contemporary hole transport materials for perovskite solar cells, Nanotechnol. Energy Environ. Eng. (2020) 145–168.

[31] A.M. Elseman, S. Sajid, A.E. Shalan, S.A. Mohamed, M.M. Rashad, Recent progress concerning inorganic hole transport layers for efficient perovskite solar cells, Appl. Phys. A Mater. Sci. Process. 125 (2019) 1–12.

[32] C. Anrango-Camacho, K. Pavón-Ipiales, B.A. Frontana-Uribe, A. Palma-Cando, Recent advances in hole-transporting layers for organic solar cells, Nanomaterials 12 (2022) 443, https://doi.org/10.3390/nano12030443.

[33] Z.Z. Sun, Y.L. Xu, W.L. Ding, W.J. Chi, How to stabilize the HOMO levels and to improve the charge transport properties of hole-transporting materials? Introducing a symmetrical core unit, Synth. Met. 247 (2019) 157–162.

[34] K. Mahmood, S. Sarwar, M.T. Mehran, Current status of electron transport layers in perovskite solar cells: materials and properties, RSC Adv. 7 (2017) 17044–17062.

[35] T. Kim, J. Lim, S. Song, Recent progress and challenges of electron transport layers in organic–inorganic perovskite solar cells, Energies 13 (2020) 5572.

[36] A. Raj, M. Kumar, A. Anshul, Recent advancement in inorganic-organic electron transport layers in perovskite solar cell: current status and future outlook, Mater. Today Chem. 22 (2021) 100595.

[37] L. Lavagna, G. Syrrokostas, L. Fagiolari, J. Amici, C. Francia, S. Bodoardo, G. Leftheriotis, F. Bella, Platinum-free photoelec-trochromic devices working with copper-based electrolytes for ultrastable smart windows, J. Mater. Chem. A 9 (2021) 19687.

[38] T. Kirchartz, P. Kaienburg, D. Baran, Figures of merit guiding research on organic solar cells, J. Phys. Chem. C 122 (2018) 5829–5843.

[39] X. Zheng, B. Chen, J. Dai, Y. Fang, Y. Bai, Y. Lin, H. Wei, X.C. Zeng, J. Huang, Defect passivation in hybrid perovskite solar cells using quaternary ammonium halide anions and cations, Nat. Energy 2 (2017) 17102.

[40] H. Chen, Z. Wei, H. He, X. Zheng, K. Sing Wong, S. Yang, H.N. Chen, Z.H. Wei, X. L. Zheng, S.H. Yang, et al., Solvent engineering boosts the efficiency of paintable carbon-based perovskite solar cells to beyond 14%, Adv. Energy Mater. 6 (2016) 1502087.

[41] N. Pellet, P. Gao, G. Gregori, T.-Y. Yang, M.K. Nazeeruddin, J. Maier, M. Grätzel, Mixed-organic-cation perovskite photo-voltaics for enhanced solar-light harvesting, Angew. Chem. Int. Ed. 53 (2014) 3151–3157.

[42] N.J. Jeon, H. Na, E.H. Jung, T.Y. Yang, Y.G. Lee, G. Kim, H.W. Shin, S. Il Seok, J. Lee, J. Seo, A fluorene-terminated hole-transporting material for highly efficient and stable perovskite solar cells, Nat. Energy 3 (2018) 682–689.

[43] J.H. Park, S.K. Hwang, S.G. Ji, J.Y. Kim, Characterization of various tandem solar cells: Protocols, issues, and precautions, Exploration (Beijing). 3 (2) (2023) 20220029, https://doi.org/10.1002/EXP.20220029. PMID: 37324037; PMCID: PMC10190969.

[44] J.P. Mailoa, C.D. Bailie, E.C. Johlin, E.T. Hoke, A.J. Akey, W.H. Nguyen, M. D. McGehee, T. Buonassisi, A 2-terminal perovskite/silicon multijunction solar cell enabled by a silicon tunnel junction, Appl. Phys. Lett. 106 (2015) 121105.

[45] H. Ko, C. Park, Y.K. Lee, Y. Jun, Recent progress in interconnection layer for hybrid photovoltaic tandems, Adv. Mater. 32 (51) (2020) 2002196.

[46] Z. Zhu, K. Mao, J. Xu, Perovskite tandem solar cells with improved efficiency and stability, J. Energy Chem. 58 (2021) 219–232.

[47] S. Akhil, S. Akash, A. Pasha, B. Kulkarni, M. Jalalah, M. Alsaiari, F.A. Harraz, R. G. Balakrishna, Review on perovskite silicon tandem solar cells: Status and prospects 2T, 3T and 4T for real world conditions, Mater. Des. 211 (2021) 110138.

[48] M.H. Futscher, B. Ehrler, Efficiency limit of perovskite/Si tandem solar cells, ACS Energy Lett. 1 (4) (2016) 863.

[49] N.N. Lal, Y. Dkhissi, W. Li, Q. Hou, Y.-B. Cheng, U. Bach, Perovskite tandem solar cells, Adv. Energy Mater. 7 (2017) 1602761.

[50] R. Sharif, A. Khalid, B. Syed, W. Ahmad, A. Rehman, H.G. Qutab, H.H. Akhtar, K. Mahmood, S. Afzal, F. Saleem, A comprehensive review of the current progresses and material advances in perovskite solar cells, Nanoscale Adv. (2023), https://doi.org/10.1039/D3NA00319A.

[51] https://www.nrel.gov/pv/cell-efficiency.html.

[52] M.A. Green, E.D. Dunlop, M. Yoshita, N. Kopidakis, K. Bothe, G. Siefer, D. Hinken, M. Rauer, J. Hohl-Ebinger, X. Hao, Solar cell efficiency tables (Version 64), Prog. Photovolt. Res. Appl. 32 (7) (2024) 425–441, https://doi.org/10.1002/pip.3831.

[53] R.K. Kothandaraman, Y. Jiang, T. Feurer, A.N. Tiwari, F. Fu, Near-infrared-transparent perovskite solar cells and perovskite-based tandem photovoltaics, Small Methods 4 (10) (2020) 2000395, https://doi.org/10.1002/smtd.202000395.

[54] S. Lu, C. Chen, J. Tang, Possible top cells for next-generation Si-based tandem solar cells, Front. Optoelectron. 13 (2020) 246–255, https://doi.org/10.1007/s12200-020-1050-y.

[55] B. Chen, Z. Yu, K. Liu, X. Zheng, Y. Liu, J. Shi, D. Spronk, P.N. Rudd, Z. Holman, J. Huang, Grain engineering for perovskite/silicon monolithic tandem solar cells with efficiency of 25.4%, Joule 3 (2019) 177–190.

[56] J. Peng, T. Duong, X. Zhou, H. Shen, Y. Wu, H.K. Mulmudi, Y. Wan, D. Zhong, J. Li, T. Tsuzuki, K.J. Weber, K.R. Catchpole, T.P. White, Efficient indium-doped TiO_x electron transport layers for high-performance perovskite solar cells and perovskite-Silicon tandems, Adv. Energy Mater. 7 (2017) 1601768.

[57] Y. Cheng, L. Ding, Perovskite/Si tandem solar cells: Fundamentals, advances, challenges, and novel applications, SusMat 1 (2021) 324–344.

[58] P. Löper, S.-J. Moon, S. Martín de Nicolas, et al., Organic–inorganic halide perovskite/crystalline silicon four-terminal tandem solar cells, Phys. Chem. Chem. Phys. 17 (2015) 1619–1629.

[59] C.D. Bailie, M.G. Christoforo, J.P. Mailoa, et al., Semi-transparent perovskite solar cells for tandems with silicon and CIGS, Energy Environ. Sci. 8 (2015) 956–963.

[60] Y. Kato, L.K. Ono, M.V. Lee, S. Wang, S.R. Raga, Y. Qi, Silver iodide formation in methyl ammonium lead iodide perovskite solar cells with silver top electrodes, Adv. Mater. Interfaces 2 (2015) 1500195.

[61] C. Bo, Y. Bai, Z. Yu, et al., Efficient semitransparent perovskite solar cells for 23.0%-efficiency perovskite/silicon four-terminal tandem cells, Adv. Energy Mater. 6 (2016) 1601128.

[62] K.A. Bush, C.D. Bailie, C. Ye, et al., Thermal and environmental stability of semi-transparent perovskite solar cells for tandems enabled by a solution-processed nanoparticle buffer layer and sputtered ITO electrode, Adv. Mater. 28 (2016) 3937–3943.

[63] T. Duong, N. Lal, D. Grant, D. Jacobs, P. Zheng, S. Rahman, H. Shen, M. Stocks, A. Blakers, K. Weber, et al., Semitransparent perovskite solar cell with sputtered front and rear electrodes for a four-terminal tandem, IEEE J. Photovolt. 6 (2016) 679–687.

[64] X. Li, D. Bi, C. Yi, J.D. Décoppet, J. Luo, S.M. Zakeeruddin, A. Hagfeldt, M. Grätzel, A vacuum flash-assisted solution process for high-efficiency large-area perovskite solar cells, Science 353 (2016) 58–62.

[65] M. Jaysankar, M. Filipič, B. Zielinski, et al., Perovskite–silicon tandem solar modules with optimised light harvesting, Energy Environ. Sci. 11 (2018) 1489–1498.

[66] C.O. Ramírez Quiroz, Y. Shen, M. Salvador, et al., Balancing electrical and optical losses for efficient 4-terminal Si–perovskite solar cells with solution processed percolation electrodes, J. Mater. Chem. A 6 (2018) 3583–3592.

[67] Z. Ren, J. Zhou, Y. Zhang, A. Ng, Q. Shen, S.H. Cheung, H. Shen, K. Li, Z. Zheng, S. K. So, Strategies for high performance perovskite/crystalline silicon four-terminal tandem solar cells, Sol. Energy Mater. Sol. Cells 179 (2018) 36–44.

[68] Z. Wang, X. Zhu, S. Zuo, et al., 27%-efficiency four-terminal perovskite/silicon tandem solar cells by sandwiched gold Nanomesh, Adv. Funct. Mater. 30 (2020) 1908298.

[69] J. Werner, L. Barraud, A. Walter, et al., Efficient near-infrared-transparent perovskite solar cells enabling direct comparison of 4-terminal and monolithic perovskite/Silicon tandem cells, ACS Energy Lett. 1 (2016) 474–480.

[70] Y. Zhang, Y. Liu, Z. Yang, S. Liu, High-quality perovskite $MAPbI_3$ single crystals for broad-spectrum and rapid response integrate photodetector, J. Energy Chem. 27 (2018) 722–727.

[71] Z.S. Yu, M. Leilaeioun, Z. Holman, Selecting tandem partners for silicon solar cells, Nat. Energy 1 (2016) 16137.

[72] A.J. Barker, A. Sadhanala, F. Deschler, M. Gandini, S.P. Senanayak, P.M. Pearce, E. Mosconi, A.J. Pearson, Y. Wu, A.R. Srimath Kandada, T. Leijtens, F. De Angelis, S.E. Dutton, A. Petrozza, R.H. Friend, Defect-assisted photoinduced halide segregation in mixed-halide perovskite thin films, ACS Energy Lett. 2 (2017) 6, https://doi.org/10.1021/acsenergylett.7b00282.

[73] K.A. Bush, K. Frohna, R. Prasanna, R.E. Beal, T. Leijtens, S.A. Swifter, M. D. McGehee, Compositional engineering for efficient wide band gap perovskites with improved stability to photoinduced phase segregation, ACS Energy Lett. 3 (2018) 428–435.

[74] X. Tang, M. Van den Berg, E. Gu, A. Horneber, G.J. Matt, A. Osvet, A.J. Meixner, D. Zhang, C.J. Brabec, Local observation of phase segregation in mixed-halide perovskite, Nano Lett. 18 (2018) 2172–2178.

[75] T. Duong, Y.L. Wu, H. Shen, et al., Rubidium multication perovskite with optimized bandgap for perovskite-silicon tandem with over 26% efficiency, Adv. Energy Mater. 7 (2017) 1700228.

[76] D.P. McMeekin, G. Sadoughi, W. Rehman, G.E. Eperon, M. Saliba, M. T. Hörantner, A. Haghighirad, N. Sakai, L. Korte, B. Rech, A mixed-cation lead mixed-halide perovskite absorber for tandem solar cells, Science 351 (2016) 151–155.

[77] S. Ašmontas, J. Gradauskas, A. Grigucevičiene, K. Leinartas, A. Lučun, M. Mujahid, K. Petrauskas, A. Selskis, A. Sužiedėlis, A. Šilenas, Triple-cation perovskite/silicon tandem solar cell, Ukr. J. Phys. Opt. 23 (2022) 193.

[78] B. Chen, S.-W. Baek, Y. Hou, E. Aydin, M. De Bastiani, B. Scheffel, A. Proppe, Z. Huang, M. Wei, Y.-K. Wang, Enhanced optical path and electron diffusion length enable high-efficiency perovskite tandems, Nat. Commun. 11 (2020) 1257.

[79] L. Yan, S. Qiu, B. Yu, J. Huang, J. Qiu, C. Zhang, F. Guo, Y. Yang, Y. Mai, Synergistic passivation of perovskite absorber films for efficient four-terminal perovskite/silicon tandem solar cells, Adv. Energy Sustain. Res. 3 (2022) 210019.

[80] Z. Fang, B. Deng, Y. Jin, et al., Surface reconstruction of wide-bandgap perovskites enables efficient perovskite/silicon tandem solar cells, Nat. Commun. 15 (2024) 10554, https://doi.org/10.1038/s41467-024-54925-4.

[81] M. Jaysankar, W. Qiu, M.V. Eerden, T. Aernouts, R. Gehlhaar, M. Debucquoy, U. W. Paetzold, J. Poortmans, Four-terminal perovskite/silicon multijunction solar modules, Adv. Energy Mater. 7 (2017) 1602807.

[82] D. Zhang, et al., Design of 4-terminal solar modules combining thin-film wide-bandgap top cells and c-Si bottom cells, Energy Proc. 77 (2015) 500–507.

[83] L. Rakocevic, et al., Interconnection optimization for highly efficient perovskite modules, IEEE J. Photovoltaics 7 (1) (2017) 404–408, https://doi.org/10.1109/JPHOTOV.2016.2626144.

[84] M. Jaysankar, S. Paetel, E. Ahlswede, U.W. Paetzold, T. Aernouts, R. Gehlhaar, J. Poortmans, Toward scalable perovskite-based multijunction solar modules, Prog. Photovoltaics Res. Appl. 27 (2019) 733–738.

[85] _September 2022: Upscaling of perovskite-silicon tandem solar cells (September 2022) conference paper.

[86] P.S.C. Schulze, K. Wienands, A.J. Bett, et al., Perovskite hybrid evaporation/spin coating method: from band gap tuning to thin film deposition on textures, Thin Solid Films 704 (2020) 137970.

[87] P.S.C. Schulze, A.J. Bett, M. Bivour, et al., 25.1% high-efficient monolithic perovskite silicon tandem solar cell with a high band gap perovskite absorber, Sol. RRL 4 (7) (2020) 2000152.

[88] T. Duong, H. Pham, T.C. Kho, et al., High efficiency perovskite-silicon tandem solar cells: effect of surface coating versus bulk incorporation of 2D perovskite, Adv. Energy Mater. 10 (2020) 1903553.

[89] S. Gharibzadeh, I.M. Hossain, P. Fassl, et al., 2D/3D heterostructure for semitransparent perovskite solar cells with engineered bandgap enables efficiencies exceeding 25% in four-terminal tandems with silicon and CIGS, Adv. Funct. Mater. 30 (2020) 1909919.

[90] D. Yang, X. Zhang, Y. Hou, K. Wang, T. Ye, J. Yoon, C. Wu, M. Sanghadasa, S. Liu, S. Priya, 28.3%-efficiency perovskite/silicon tandem solar cell by optimal transparent electrode for high efficient semitransparent top cell, Nano Energy 84 (2021) 105934.

[91] T. Huang, R. Wang, S. Nuryyeva, S. Tan, J. Xue, Y. Zhao, Q. Wu, M.H. Weber, P. Cheng, D. Meng, I. Yavuz, K.N. Houk, Y. Yang, Wide-gap perovskite via synergetic surface passivation and its application toward efficient stacked tandem photovoltaics, Small 18 (2022) 1–9.

[92] Shukla N, Verma A. K, Tiwari S. Optimization of Efficient Perovskite-Si Hybrid Tandem Solar Cells. Mat. Sci. Res. India; 20(1).

[93] S.D.H. Naqvi, K. Son, W. Jung, H.U. Hwang, S. Lee, A. Lee, M. Keum, S. Kim, J. W. Kim, M.G. Kang, et al., Mitigating intrinsic interfacial degradation in semi-transparent perovskite solar cells for high efficiency and long-term stability, Adv. Energy Mater. 13 (2023) 2302147.

[94] W. Chai, L. Li, W. Zhu, D. Chen, L. Zhou, H. Xi, J. Zhang, C. Zhang, Y. Hao, Graded heterojunction improves wide-bandgap perovskite for highly efficient 4-terminal perovskite/silicon tandem solar cells, Research 6 (2023) 196.

[95] T. Duong, T. Nguyen, K. Huang, H. Pham, S.G. Adhikari, M.R. Khan, L. Duan, W. Liang, K.C. Fong, H. Shen, et al., Bulk incorporation with 4-methylphene-thylammonium chloride for efficient and stable methylammonium-free perovskite and perovskite-silicon tandem solar cells, Adv. Energy Mater. 13 (2023) 2203607.

[96] Z. Li, X. Li, X. Chen, X. Cui, C. Guo, X. Feng, D. Ren, Y. Mo, M. Yang, H. Huang, et al., In situ epitaxial growth of blocking structure in mixed-halide wide-band-gap perovskites for efficient photovoltaics, Joule 7 (2023) 1363–1381.

[97] J. Tao, J. Xue, H. Guo, Y. Wang, J. Shen, T. Wang, T. He, G. Fu, S. Yang, Precisely adjusting the organic/electrode interface charge barrier for efficient and stable ag-based regular perovskite solar cells with >23% efficiency, Chem. Eng. J. 463 (2023) 142445.

[98] Y. Ou, H. Huang, H. Shi, Z. Li, Z. Chen, M. Mateen, Z. Lu, D. Chi, S. Huang, Collaborative interfacial modification and surficial passivation for high-efficiency MA-free wide-bandgap perovskite solar cells, Chem. Eng. J. 469 (2023) 143860.
[99] F. Sahli, B.A. Kamino, J. Werner, et al., Improved optics in monolithic perovskite/silicon tandem solar cells with a nanocrystalline silicon recombination junction, Adv. Energy Mater. 8 (2018) 1701609.
[100] F. Sahli, J. Werner, B.A. Kamino, et al., Fully textured monolithic perovskite/silicon tandem solar cells with 25.2% power conversion efficiency, Nat. Mater. 17 (2018) 820–826.
[101] L. Mazzarella, Y.-H. Lin, S. Kirner, et al., Infrared light management using a nanocrystalline silicon oxide interlayer in monolithic perovskite/silicon heterojunction tandem solar cells with efficiency above 25%, Adv. Energy Mater. 9 (2019) 1803241.
[102] Z. Ying, Z. Yang, J. Zheng, H. Wei, L. Chen, C. Xiao, J. Sun, C. Shou, G. Qin, J. Sheng, et al., Monolithic perovskite/black-silicon tandems based on tunnel oxide passivated contacts, Joule 6 (2022) 2644–2661.
[103] E. Köhnen, P. Wagner, F. Lang, A. Cruz, B. Li, M. Rob, M. Jost, A.B. Morales-Vilches, M. Topic, M. Stolterfoht, et al., 27.9% efficient monolithic perovskite/silicon tandem solar cells on industry compatible bottom cells, Sol. RRL 5 (2021) 2100244.
[104] S. Albrecht, M. Saliba, J.P. Correa Baena, F. Lang, L. Kegelmann, M. Mews, L. Steier, A. Abate, J. Rappich, L. Korte, et al., Monolithic perovskite/silicon-heterojunction tandem solar cells processed at low temperature, Energy Environ. Sci. 9 (2016) 81–88.
[105] G. Kakavelakis, T. Maksudov, D. Konios, I. Paradisanos, G. Kioseoglou, E. Stratakis, E. Kymakis, Efficient and highly air stable planar inverted perovskite solar cells with reduced graphene oxide doped PCBM Electron transporting layer, Adv. Energy Mater. 7 (2016) 1602120.
[106] J. Werner, C.H. Weng, A. Walter, L. Fesquet, J.P. Seif, S. De Wolf, B. Niesen, C. Ballif, Efficient monolithic perovskite/silicon tandem solar cell with cell area >1 cm^2, J. Phys. Chem. Lett. 7 (2016) 161–166.
[107] Y.L. Wu, D. Yan, J. Peng, et al., Monolithic perovskite/silicon-homojunction tandem solar cell with over 22% efficiency, Energy Environ. Sci. 10 (2017) 2472–2479.
[108] J. Zheng, C.F.J. Lau, H. Mehrvarz, et al., Large area efficient interface layer free monolithic perovskite/homo-junction-silicon tandem solar cell with over 20% efficiency, Energy Environ. Sci. 11 (2018) 2432–2443.
[109] H. Shen, S.T. Omelchenko, D.A. Jacobs, et al., In situ recombination junction between p-Si and TiO_2 enables high-efficiency monolithic perovskite/Si tandem cells, Sci. Adv. 4 (2018) eaau9711.
[110] G. Nogay, F. Sahli, J. Werner, et al., 25.1%-efficient monolithic perovskite/silicon tandem solar cell based on a p-type monocrystalline textured silicon wafer and high-temperature passivating contacts, ACS Energy Lett. 4 (2019) 844–845.
[111] C.U. Kim, J.C. Yu, E.D. Jung, et al., Optimization of device design for low cost and high efficiency planar monolithic perovskite/silicon tandem solar cells, Nano Energy 60 (2019) 213–221.
[112] Z. Qiu, Z. Xu, N. Li, et al., Monolithic perovskite/Si tandem solar cells exceeding 22% efficiency via optimizing top cell absorber, Nano Energy 53 (2018) 798–807.
[113] E. Köhnen, M. Jošt, A. Belen Morales-Vilches, P. Tockhorn, A. Al-Ashouri, B. Macco, L. Kegelmann, L. Korte, B. Rech, R. Schlatmann, et al., Highly efficient monolithic perovskite silicon tandem solar cells: Analyzing the influence of current mismatch on device performance, Science 367 (2020) 1135–1140.
[114] A. Al-Ashouri, E. Köhnen, B. Li, A. Magomedov, H. Hempe, P. Caprioglio, J. A. Marquez, A.B. Morales-Vilches, E. Kasparavicius, J.A. Smith, et al., Monolithic perovskite/silicon tandem solar cell with >29% efficiency by enhanced hole extraction, Science 370 (2020) 1300–1309.
[115] J. Xu, C.C. Boyd, Z.J. Yu, A.F. Palmstrom, D.J. Witter, D.J. Larson, R.M. France, J. Werner, S.P. Harvey, E.J. Wolf, et al., Triple-halide wide–band gap perovskites with suppressed phase segregation for efficient tandems, Science 367 (2020) 1097–1104.
[116] Y. Hou, E. Aydin, M. De Bastiani, et al., Efficient tandem solar cells with solution-processed perovskite on textured crystalline silicon, Science 367 (2020) 1135–1140.
[117] K. Masuko, M. Shigematsu, T. Hashiguchi, D. Fujishima, M. Kai, N. Yoshimura, T. Yamaguchi, Y. Ichihashi, T. Mishima, N. Matsubara, et al., Achievement of more than 25% conversion efficiency with crystalline silicon heterojunction solar cell, IEEE J. Photovolt. 4 (2014) 1433–1435 (CLOSED).
[118] T. Mishima, M. Taguchi, H. Sakata, E. Maruyama, Development status of high-efficiency HIT solar cells, Sol. Energy Mater. Sol. Cells 95 (2011) 18–21.
[119] A. Razzaq, T.G. Allen, W. Liu, Z. Liu, S. De Wolf, Silicon heterojunction solar cells: Techno-economic assessment and opportunities, Joule 6 (2022) 514–542.
[120] D. Turkay, K. Artuk, X. Chin, D.A. Jacobs, S. Moon, A. Walter, M. Mensi, G. Andreatta, N. Blondiaux, H. Lai, F. Fu, M. Boccard, Q. Jeangros, C.M. Wolff, C. Ballif, Synergetic substrate and additive engineering for over 30%-efficient perovskite-Si tandem solar cells, Joule 8 (6) (2024) 1735–1753, https://doi.org/10.1016/j.joule.2024.04.015.
[121] D. Kim, H.J. Jung, I.J. Park, B.W. Larson, S.P. Dunfield, C. Xiao, J. Kim, J. Tong, P. Boonmongkolras, S.G. Ji, et al., Efficient, stable silicon tandem cells enabled by anion-engineered wide-bandgap perovskites, Science 368 (2020) 155–160.
[122] K.A. Bush, A.F. Palmstrom, Z.S.J. Yu, M. Boccard, R. Cheacharoen, J.P. Mailoa, D. P. McMeekin, R.L.Z. Hoye, C.D. Bailie, T. Leijtens, I.M. Peters, M.C. Minichetti, N. Rolston, R. Prasanna, S. Sofia, D. Harwood, W. Ma, F. Moghadam, H.J. Snaith, T. Buonassisi, Z.C. Holman, S.F. Bent, M.D. McGehee, 23.6%-efficient monolithic perovskite/silicon tandem solar cells with improved stability, Nat. Energy 2 (2017) 17009.
[123] J. Zheng, H. Mehrvarz, F.-J. Ma, et al., 21.8% efficient monolithic perovskite/homo-junction-silicon tandem solar cell on 16 cm^2, ACS Energy Lett. 3 (2018) 2299–2300.
[124] K.A. Bush, S. Manzoor, K. Frohna, et al., Minimizing current and voltage losses to reach 25% efficient monolithic two-terminal perovskite–silicon tandem solar cells, ACS Energy Lett. 3 (2018) 2173–2180.
[125] B. Chen, Z.J. Yu, S. Manzoor, S. Wang, W. Weigand, Z. Yu, G. Yang, Z. Ni, X. Dai, Z.C. Homan, et al., Blade-coated perovskites on textured silicon for 26%-efficient monolithic perovskite/silicon tandem solar cells, Joule 4 (2020) 850–864.
[126] M. Roß, S. Severin, M.B. Stutz, P. Wagner, H. Köbler, M. Favin-Leveque, A. Al-Ashouri, P. Korb, P. Tockhorn, A. Abate, et al., Co-evaporated Formamidinium lead iodide based perovskites with 1000 h constant stability for fully textured monolithic perovskite/silicon tandem solar cells, Adv. Energy Mater. 11 (2021) 2101460.
[127] F.H. Isikgor, F. Furlan, J. Liu, E. Ugur, M.K. Eswaran, A.S. Subbiah, E. Yengel, M. De Bastiani, G.T. Harrison, S. Zhumagali, et al., Concurrent cationic and anionic perovskite defect passivation enables 27.4% perovskite/silicon tandems with suppression of halide segregation, Joule 5 (2021) 1566–1586.
[128] S. Zhumagali, F.H. Isikgor, P. Maity, J. Yin, E. Ugur, M. De Bastiani, A.S. Subbiah, A.J. Mirabelli, R. Azmi, G.T. Harrison, et al., Linked nickel oxide/perovskite interface passivation for high-performance textured monolithic tandem solar cells, Adv. Energy Mater. 11 (2021) 2101662.
[129] R. Santbergen, M.R. Vogt, R. Mishima, M. Hino, H. Uzu, D. Adachi, K. Yamamoto, M. Zeman, O. Isabella, Ray-optics study of gentle non-conformal texture morphologies for perovskite/silicon tandems, Opt. Express 30 (2022) 5608–5617.
[130] P. Tockhorn, J. Sutter, A. Cruz, P. Wagner, K. Jäger, D. Yoo, F. Lang, M. Grischek, B. Li, J. Li, et al., Nano-optical designs for high-efficiency monolithic perovskite–silicon tandem solar cells, Nat. Nanotechnol. 17 (2022) 1214–1221.
[131] C. Hsieh, J. Huang, Y. Wu, Analysis of two-terminal perovskite/silicon tandem solar cells with differing texture structure, perovskite carrier lifetime and tunneling junction quality, ArXiv. Doi 10 (1063/5) (2023) 0193641.
[132] J. Zheng, W. Duan, Y. Guo, Z.C. Zhao, H. Yi, F.-J. Ma, L. Granados Caro, C. Yi, J. Bing, S. Tang, et al., Efficient monolithic perovskite–Si tandem solar cells enabled by an ultra-thin indium tin oxide interlayer, Energy Environ. Sci. 16 (2023) 1223–1233.
[133] P. Hang, C. Kan, B. Li, Y. Yao, Z. Hu, Y. Zhang, J. Xie, Y. Wang, D. Yang, X. Yu, Highly efficient and stable wide-bandgap perovskite solar cells via strain management, Adv. Funct. Mater. 33 (2023) 2214381.
[134] X. Li, Z. Ying, J. Zheng, X. Wang, Y. Chen, M. Wu, C. Xiao, J. Sun, C. Shou, Z. Yang, Y. Zeng, X. Yang, J. Ye, Surface reconstruction for efficient and stable monolithic perovskite/silicon tandem solar cells with greatly suppressed residual strain, Adv. Mater. 35 (30) (2023) 2211962, https://doi.org/10.1002/adma.202211962.
[135] X.Y. Chin, D. Turkay, J.A. Steele, S. Tabean, S. Eswara, M. Mensi, P. Fiala, C. M. Wolff, A. Paracchino, K. Artuk, D. Jacobs, Q. Guesnay, F. Sahli, G. Andreatta, M. Boccard, Q. Jeangros, C. Ballif, Interface passivation for 31.25%-efficient perovskite/silicon tandem solar cells, Science 381 (6653) (2023) 59–63, https://doi.org/10.1126/science.adg0091. Epub 2023 Jul 6. PMID: 37410835.
[136] J. Zheng, Z. Ying, Z. Yang, Z. Lin, H. Wei, L. Chen, X. Yang, Y. Zeng, X. Li, J. Ye, Polycrystalline silicon tunnelling recombination layers for high-efficiency perovskite/tunnel oxide passivating contact tandem solar cells, Nat. Energy 8 (11) (2023) 1250–1261, https://doi.org/10.1038/s41560-023-01382-w.
[137] G. Wang, J. Zheng, W. Duan, J. Yang, M.A. Mahmud, Q. Lian, S. Tang, C. Liao, J. Bing, J. Yi, T.L. Leung, X. Cui, H. Chen, F. Jiang, Y. Huang, A. Lambertz, M. Jankovec, M. Topič, S. Bremner, A. Ho-Baillie, Molecular engineering of hole-selective layer for high band gap perovskites for highly efficient and stable perovskite-silicon tandem solar cells, Joule 7 (11) (2023) 2583–2594, https://doi.org/10.1016/j.joule.2023.09.007.
[138] H. Luo, X. Zheng, W. Kong, Z. Liu, H. Li, J. Wen, R. Xia, H. Sun, P. Wu, Y. Wang, et al., Inorganic framework composition engineering for scalable fabrication of perovskite/silicon tandem solar cells, ACS Energy Lett. 8 (2023) 4993–5002.
[139] J. Liu, B. Shi, Q. Xu, et al., Textured perovskite/silicon tandem solar cells achieving over 30% efficiency promoted by 4-fluorobenzylamine hydroiodide, Nano-Micro Lett. 16 (2024) 189, https://doi.org/10.1007/s40820-024-01406-4.
[140] Perovskite solar cell – Wikipedia Url: https://en.wikipedia.org/wiki/Perovskite_solar_cell. Website.
[141] H. Shen, T. Duong, J. Peng, D. Jacobs, N. Wu, J. Gong, Y. Wu, S.K. Karuturi, X. Fu, K. Weber, X. Xiao, T.P. White, K. Catchpole, Mechanically-stacked perovskite/CIGS tandem solar cells with efficiency of 23.9% and reduced oxygen sensitivity, Energy Environ. Sci. 11 (2018) 394–406.
[142] M. Wright, et al., Design considerations for the bottom cell in perovskite/silicon tandems: a terawatt scalability perspective, Energy Environ. Sci. 16 (10) (2023) 4164–4190.
[143] W. Akram, et al., A review of life cycle assessment and sustainability analysis of perovskite/Si tandem solar cells, Energy Environ. Sci. 3 (2025) 21–36.
[144] S. Bremner, C. Yi, I. Almansouri, A. Ho-Baillie, M. Green, Optimum band gap combinations to make best use of new photovoltaic materials, Sol. Energy 135 (2016) 750–757.
[145] A. Babayigit, A. Ethirajan, M. Muller, et al., Toxicity of organometal halide perovskite solar cells, Nature Mater 15 (2016) 247–251, https://doi.org/10.1038/nmat4572.
[146] B. Nejand, S. Gharibzadeh, V. Ahmadi, et al., Novel solvent-free perovskite deposition in fabrication of normal and inverted architectures of perovskite solar cells, Sci. Rep. 6 (2016) 33649, https://doi.org/10.1038/srep33649.
[147] B. Hailegnaw, S. Kirmayer, E. Edri, G. Hodes, D. Cahen, Rain on methylammonium lead iodide based perovskites: possible environmental effects

of perovskite solar cells, J. Phys. Chem. Lett. 6 (9) (2015) 1543–1547, https://doi.org/10.1021/acs.jpclett.5b00504.
[148] A. Babayigit, D. Duy Thanh, A. Ethirajan, et al., Assessing the toxicity of Pb- and Sn-based perovskite solar cells in model organism *Danio rerio*, Sci. Rep. 6 (2016) 18721, https://doi.org/10.1038/srep18721.
[149] M.A. Scarpulla, B. McCandless, A.B. Phillips, Y. Yan, M.J. Heben, C. Wolden, G. Xiong, W.K. Metzger, D. Mao, D. Krasikov, I. Sankin, S. Grover, A. Munshi, W. Sampath, J.R. Sites, A. Bothwell, D. Albin, M.O. Reese, A. Romeo, S.M. Hayes, CdTe-based thin film photovoltaics: recent advances, current challenges and future prospects, Sol. Energy Mater. Sol. Cells 255 (2023) 112289, https://doi.org/10.1016/j.solmat.2023.112289.
[150] Y. Jiang, L. Qiu, E.J. Juarez-Perez, L.K. Ono, Z. Hu, Z. Liu, Z. Wu, L. Meng, Q. Wang, Y. Qi, Reduction of lead leakage from damaged lead halide perovskite solar modules using self− healing polymer−based encapsulation, Nat. Energy 4 (2019) 585–593.
[151] K. Aitola, G. Gava Sonai, M. Markkanen, J. Jaqueline Kaschuk, X. Hou, K. Miettunen, P.D. Lund, Encapsulation of commercial and emerging solar cells with focus on perovskite solar cells, Sol. Energy 237 (2022) 264–283, https://doi.org/10.1016/j.solener.2022.03.060.
[152] Li, C.; Huang, W.; Gao, L.; Wang, H.; Hu, L.; Chen, T.; Zhang, H. Nanoscale 2020, 12, (4), 2201-2227. [Recent advances in solution-processed photodetectors based on inorganic and hybrid photo-active materials].
[153] K. Nishimura, M.A. Kamarudin, D. Hirotani, et al., Lead-free tin-halide perovskite solar cells with 13% efficiency, Nano Energy 74 (2020) 104858.
[154] C. Zuo, L. Ding, Lead-free perovskite materials $(NH_4)_3Sb_2I_xBr_{9-x}$, Angew. Chem. Int. Ed. 56 (2017) 6528–6532.
[155] Z. Fang, S. Wang, S. Yang, et al., $CsAg_2Sb_2I_9$ solar cells, Inorg. Chem. Front. 5 (2018) 1690–1693.
[156] W. Hu, X. He, Z. Fang, et al., Bulk heterojunction gifts bismuth-based lead-free perovskite solar cells with record efficiency, Nano Energy 68 (2020) 104362.
[157] X.-G. Zhao, J.-H. Yang, Y. Fu, et al., Design of lead-free inorganic halide perovskites for solar cells via cation-transmutation, J. Am. Chem. Soc. 139 (2017) 2630–2638.
[158] W. Ke, M.G. Kanatzidis, Prospects for low-toxicity lead-free perovskite solar cells, Nat. Commun. 10 (2019) 965, https://doi.org/10.1038/s41467-019-08918-3. Or Ke, W.; Kanatzidis, M. G. J. N. c. 2019, 10, (1), 1-4.
[159] Y. Jiang, M.R. Leyden, L. Qiu, S. Wang, L.K. Ono, Z. Wu, E.J. Juarez-Perez, Y. Qi, Combination of hybrid CVD and cation exchange for upscaling Cs-substituted mixed cation perovskite solar cells with high efficiency and stability, Adv. Funct. Mater. 28 (1) (2017) 1703835, https://doi.org/10.1002/adfm.201703835.
[160] Z. Li, T.R. Klein, D.H. Kim, M. Yang, J.J. Berry, M.F.A.M. van Hest, K. Zhu, Scalable fabrication of perovskite solar cells, Nat. Rev. Mater. 3 (2018) 18017.
[161] R. Swartwout, M.T. Hoerantner, V. Bulović, Scalable deposition methods for large-area production of perovskite thin films, Energy & Environmental Materials 2 (2) (2019) 119–145, https://doi.org/10.1002/eem2.12043.
[162] S.Y. Chen, A. Walsh, J.H. Yang, X.G. Gong, L. Sun, P.X. Yang, J.H. Chu, S.H. Wei, Compositional dependence of structural and electronic properties of $Cu_2ZnSn(S,Se)_4$ alloys for thin film solar cells, Phys. Rev. B: Condens. Matter Mater. Phys. 83 (2011) 125201.
[163] X. Dai, Y. Deng, C.H. Van Brackle, J. Huang, Meniscus fabrication of halide perovskite thin films at high throughput for large area and low-cost solar panels, Int. J. Extrem. Manuf. 1 (2019) 022004.
[164] Y. Liu, L.A. Renna, M. Bag, et al., High efficiency tandem thin-perovskite/polymer solar cells with a graded recombination layer, ACS Appl. Mater. Interfaces 8 (2016) 7070–7076.
[165] X. Chen, Z. Jia, Z. Chen, et al., Efficient and reproducible monolithic perovskite/organic tandem solar cells with low-loss interconnecting layers, Joule 4 (2020) 1594–1606.
[166] Q. Zeng, L. Liu, Z. Xiao, et al., A two-terminal all-inorganic perovskite/organic tandem solar cell, Sci. Bull. 64 (2019) 885–887.
[167] A.F. Palmstrom, G.E. Eperon, T. Leijtens, R. Prasanna, S.N. Habisreutinger, W. Nemeth, E.A. Gaulding, S.P. Dunfield, M. Reese, S. Nanayakkara, et al., Enabling flexible all-perovskite tandem solar, Joule 3 (9) (2019) 2193–2204.
[168] F. Fu, T. Feurer, T. Jäger, et al., Low-temperature-processed efficient semi-transparent planar perovskite solar cells for bifacial and tandem applications, Nat. Commun. 6 (2015) 8932.
[169] F. Fu, T. Feurer, T. Weiss, et al., High-efficiency inverted semi-transparent planar perovskite solar cells in substrate configuration, Nat. Energy 2 (2017) 16190.
[170] D.H. Kim, C.P. Muzzillo, J. Tong, A.F. Palmstrom, B.W. Larson, C. Choi, S. P. Harvey, S. Glynn, J.B. Whitaker, F. Zhang, et al., Bimolecular additives improve wide-band-gap perovskites for efficient tandem solar cells with CIGS, Joule 3 (2019) 1734–1745.
[171] T. Feurer, R. Carron, G. Torres Sevilla, F. Fu, S. Pisoni, Y.E. Romanyuk, S. Buecheler, A.N. Tiwari, Efficiency improvement of near-stoichiometric $CuInSe_2$ solar cells for application in tandem devices, Adv. Energy Mater. 9 (2019) 2–7.
[172] M.A. Green, K. Emery, Y. Hishikawa, W. Warta, E.D. Dunlop, Solar cell efficiency tables (version 48), Prog. Photovolt. Res. Appl. 24 (7) (2016) 905–913, https://doi.org/10.1002/pip.2788. Or Green, M. A. J. N. E. 2016, 1, (1), 1-4.
[173] M.A. Green, Commercial progress and challenges for photovoltaics, Nat. Energy 1 (2016) 15015.
[174] Razera, R. A.; Jacobs, D. A.; Fu, F.; Fiala, P.; Dussouillez, M.; Sahli, F.; Yang, T. C.; Ding, L.; Walter, A.; Feil, A. F. J. J. o. M. C. A. 2020, 8, (1), 242-250. [Instability of p–i–n perovskite solar cells under reverse bias].
[175] F. Li, M. Liu, Recent efficient strategies for improving the moisture stability of perovskite solar cells, J. Mater. Chem. A 5 (2017) 15447–15459.
[176] R. Wang, M. Mujahid, Y. Duan, Z.K. Wang, J. Xue, Y. Yang, A review of perovskites solar cell stability, Adv. Funct. Mater. 29 (2019) 1808843.
[177] E.J. Juarez-Perez, Z. Hawash, S.R. Raga, L.K. Ono, Y. Qi, Thermal degradation of $CH_3NH_3PbI_3$ perovskite into NH_3 and CH_3I gases observed by coupled thermogravimetry–mass spectrometry analysis, Energy Environ. Sci. 9 (2016) 3406–3410.
[178] Y. Yuan, J. Huang, Ion migration in organometal trihalide perovskite and its impact on photovoltaic efficiency and stability, Acc. Chem. Res. 49 (2016) 286–293.
[179] J. Mizusaki, K. Arai, K. Fueki, Ionic conduction of the perovskite-type halides, Solid State Ion. 11 (1983) 203–211.
[180] E. Bi, H. Chen, F. Xie, Y. Wu, W. Chen, Y. Su, A. Islam, M. Grätzel, X. Yang, L. Han, Diffusion engineering of ions and charge carriers for stable efficient perovskite solar cells, Nat. Commun. 8 (2017) 15330.
[181] Z. Yang, B.H. Babu, S. Wu, T. Liu, S. Fang, Z. Xiong, L. Han, W. Chen, Review on practical interface engineering of perovskite solar cells: from efficiency to stability, Sol. RRL 4 (2020) 1900257.
[182] B. Conings, J. Drijkoningen, N. Gauquelin, A. Babayigit, J. D'Haen, L. D'Olieslaeger, A. Ethirajan, J. Verbeeck, J. Manca, E. Mosconi, Intrinsic thermal instability of methylammonium lead trihalide perovskite, Adv. Energy Mater. 5 (2015) 1500477.
[183] M.S. Islam, Computer modelling of defects and transport in perovskite oxides, Solid State Ion. 154–155 (2002) 75–85.
[184] A. Walsh, C.R.A. Catlow, A.G.H. Smith, A.A. Sokol, S.M. Woodley, Strontium migration assisted by oxygen vacancies in $SrTiO_3$ from classical and quantum mechanical simulations, Phys. Rev. B 83 (2011) 220301.
[185] H.J. Snaith, A. Abate, J.M. Ball, G.E. Eperon, T. Leijtens, N.K. Noel, S.D. Stranks, J.-T.-W. Wang, K. Wojciechowski, W. Zhang, Anomalous hysteresis in perovskite solar cells, J. Phys. Chem. Lett. 5 (2014) 1511–1515.
[186] W. Tress, N. Marinova, T. Moehl, S.M. Zakeeruddin, M.K. Nazeeruddin, M. Grätzel, Understanding the rate-dependent J–V hysteresis, slow time component, and aging in $CH_3NH_3PbI_3$ perovskite solar cells: the role of a compensated electric field, Energy Environ. Sci. 8 (2015) 995–1004.
[187] H.-S. Kim, N.-G. Park, Parameters affecting I–V hysteresis of $CH_3NH_3PbI_3$ perovskite solar cells: Effects of perovskite crystal size and mesoporous TiO_2 layer, J. Phys. Chem. Lett. 5 (2014) 2927–2934.
[188] K. Cao, H. Li, S. Liu, J. Cui, Y. Shen, M. Wang, $MAPbI_{3-x}Br_x$ mixed halide perovskites for fully printable mesoscopic solar cells with enhanced efficiency and less hysteresis, Nanoscale 8 (2016) 8839–8846.
[189] J.H. Heo, H.J. Han, D. Kim, T.K. Ahn, S.H. Im, Hysteresis-less inverted $CH_3NH_3PbI_3$ planar perovskite hybrid solar cells with 18.1% power conversion efficiency, Energy Environ. Sci. 8 (2015) 1602–1608.
[190] C.-G. Wu, C.-H. Chiang, Z.-L. Tseng, M.K. Nazeeruddin, A. Hagfeldt, M. Grätzel, High efficiency stable inverted perovskite solar cells without current hysteresis, Energy Environ. Sci. 8 (2015) 2725–2733.
[191] E.L. Unger, E.T. Hoke, C.D. Bailie, W.H. Nguyen, A.R. Bowring, T. Heumüller, M. G. Christoforo, M.D. McGehee, Hysteresis and transient behavior in current–voltage measurements of hybrid-perovskite absorber solar cells, Energy Environ. Sci. 7 (2014) 3690–3698.
[192] S.-H. Turren-Cruz, A. Hagfeldt, M. Saliba, Methylammonium-free, high-performance, and stable perovskite solar cells on a planar architecture, Science 362 (2018) 449–453.
[193] M. Saliba, T. Matsui, J.-Y. Seo, K. Domanski, J.-P. Correa-Baena, M. K. Nazeeruddin, S.M. Zakeeruddin, W. Tress, A. Abate, A. Hagfeldt, Cesium-containing triple cation perovskite solar cells: improved stability, reproducibility and high efficiency, Energy Environ. Sci. 9 (2016) 1989–1997.
[194] C. Yi, J. Luo, S. Meloni, et al., Entropic stabilization of mixed A-cation ABX_3 metal halide perovskites for high performance perovskite solar cells, Energy Environ. Sci. 9 (2016) 656–662.
[195] P. Gao, A.R. Bin Mohd Yusoff, M.K. Nazeeruddin, Dimensionality engineering of hybrid halide perovskite light absorbers, Nat. Commun. 9 (2018) 5028.
[196] X. Hu, J. Li, C. Wang, et al., Antimony potassium tartrate stabilizes wide-bandgap perovskites for inverted 4-T all-perovskite tandem solar cells with efficiencies over 26%, Nano-Micro Lett. 15 (2023) 103, https://doi.org/10.1007/s40820-023-01078-6.
[197] M. Saliba, T. Matsui, K. Domanski, J.-Y. Seo, A. Ummadisingu, S.M. Zakeeruddin, J.-P. Correa-Baena, W.R. Tress, A. Abate, A.J.S. Hagfeldt, Incorporation of rubidium cations into perovskite solar cells improves photovoltaic performance, Science 354 (2016) 206–209.
[198] J. Huang, P. Xu, J. Liu, X.Z. You, Sequential introduction of cations deriving large-grain $Cs_xFA_{1-x}PbI_3$ thin film for planar hybrid solar cells: insight into phase-segregation and thermal-healing behavior, Small 13 (2017) 1603225.
[199] T. Duong, H.K. Mulmudi, H. Shen, Y. Wu, C. Barugkin, Y.O. Mayon, H.T. Nguyen, D. Macdonald, J. Peng, M. Lockrey, Structural engineering using rubidium iodide as a dopant under excess lead iodide conditions for high efficiency and stable perovskites, Nano Energy 30 (2016) 330–340.
[200] M. Abdi-Jalebi, Z. Andaji-Garmaroudi, A.J. Pearson, G. Divitini, S. Cacovich, B. Philippe, H. Rensmo, C. Ducati, R.H. Friend, S.D. Stranks, Potassium- and rubidium-passivated alloyed perovskite films: optoelectronic properties and moisture stability, ACS Energy Lett. 3 (2018) 2671–2678.
[201] J.W. Lee, D.H. Kim, H.S. Kim, S.W. Seo, S.M. Cho, N.G. Park, Formamidinium and cesium hybridization for photo-and moisture-stable perovskite solar cell, Adv. Energy Mater. 5 (2015) 1501310.
[202] J. Chen, W.C. Choy, Efficient and stable all-inorganic perovskite solar cells, Sol. RRL 4 (2020) 2000408.

[203] Z. Song, C. Chen, C. Li, et al., Wide-bandgap, low-bandgap, and tandem perovskite solar cells, Semicond. Sci. Technol. 34 (2019) 093001.
[204] Z. Yang, A. Rajagopal, S.B. Jo, C.-C. Chueh, S. Williams, C.-C. Huang, J. K. Katahara, H.W. Hillhouse, A.K.Y. Jen, Stabilized wide bandgap perovskite solar cells by tin substitution, Nano Lett. 16 (2016) 7739–7747.
[205] M. Abdi-Jalebi, Z. Andaji-Garmaroudi, S. Cacovich, C. Stavrakas, B. Philippe, J. M. Richter, M. Alsari, E.P. Booker, E.M. Hutter, A.J. Pearson, S. Lilliu, T. J. Savenije, H. Rensmo, G. Divitini, C. Ducati, R.H. Friend, S.D. Stranks, Maximizing and stabilizing luminescence from halide perovskites with potassium passivation, Nature 555 (2018) 497.
[206] P. Wang, X. Zhang, Y. Zhou, et al., Solvent-controlled growth of inorganic perovskite films in dry environment for efficient and stable solar cells, Nat. Commun. 9 (2018) 2225.
[207] X. Jia, L. Liu, Z. Fang, TBAB additive for inorganic $CsPbI_{2.4}Br_{0.6}$ perovskite solar cells with efficiency beyond 15%, J. Mater. Chem. C 7 (2019) 7207–7211.
[208] B. Zhao, S.-F. Jin, S. Huang, N. Liu, J.-Y. Ma, D.-J. Xue, Q. Han, J. Ding, Q.-Q. Ge, Y. Feng, Thermodynamically stable orthorhombic γ-$CsPbI_3$ thin films for high-performance photovoltaics, J. Am. Chem. Soc. 140 (2018) 11716–11725.
[209] Y. Wang, T. Zhang, M. Kan, et al., Bifunctional stabilization of all-inorganic a$CsPbI_3$ perovskite for 17% efficiency photovoltaics, J. Am. Chem. Soc. 140 (2018) 12345–12348.
[210] Z. Fang, L. Liu, Z. Zhang, et al., $CsPbI_{2.25}Br_{0.75}$ solar cells with 15.9% efficiency. Sci, Bull. Georgian Acad. Sci. 64 (2019) 507–510.
[211] W. Zhou, Z. Wen, P. Gao, Less is more: dopant-free hole transporting materials for high-efficiency perovskite solar cells, Adv. Energy Mater. 8 (2018) 1702512.
[212] K. Domanski, J.-P. Correa-Baena, N. Mine, et al., Not all that glitters is gold: metal-migration-induced degradation in perovskite solar cells, ACS Nano 10 (2016) 6306–6314.
[213] L. Zhao, R.A. Kerner, Z. Xiao, et al., Redox chemistry dominates the degradation and decomposition of metal halide perovskite optoelectronic devices, ACS Energy Lett. 1 (2016) 595–602.
[214] B. Chen, N. Ren, Y. Li, L. Yan, S. Mazumdar, Y. Zhao, X. Zhang, Insights into the development of monolithic perovskite/silicon tandem solar cells, Adv. Energy Mater. 12 (2022) 2003628.
[215] M. Shahinuzzaman, S. Afroz, H. Mohafez, M.S. Jamal, M.U. Khandaker, A. Sulieman, N. Tamam, M.A. Islam, Roles of inorganic oxide based HTMs towards highly efficient and long-term stable PSC—a review, Nanomaterials 12 (17) (2022) 3003.